Spatial transcriptional signatures define margin morphogenesis along the proximal-distal and medio-lateral axes in complex leaf species *Solanum lycopersicum* (tomato)

Authors: Ciera C. Martinez[1,2,3], Siyu Li[3], Margaret R. Woodhouse[3], Keiko Sugimoto[4], and Neelima R. Sinha[3*]

[1]Department of Molecular and Cellular Biology, University of California at Berkeley, Berkeley, CA 94709, USA
[2]Berkeley Institute of Data Science, University of California at Berkeley, Berkeley, CA 94709, USA
[3]Department of Plant Biology, University of California at Davis, Davis, CA 95616, USA
[4]RIKEN Center for Sustainable Resource Science, Tsurumi, Yokohama, 15 230-0045 Japan
*Author for correspondence

ABSTRACT

Plant morphogenesis is achieved by an interplay among the processes of cell differentiation, elongation, and specialization. During leaf development cells proceed through these processes at different rates depending on position along the medio-lateral and proximal-distal axes of the organ. The gene expression changes controlling cell fate along these axes remained elusive due to the difficulties in precise tissue isolation. This study combines rigorous early leaf characterization, laser capture microdissection, and transcriptomic sequencing to ask how patterns of gene expression regulate early leaf morphogenesis along the medio-lateral and proximal-distal axes in wild type *Solanum lycopersium* (tomato) and a leaf morphogenetic mutant *trifoliate* (*tf-2*). This work reveals transcriptional regulation of cell differentiation patterning along the proximal distal axis, and also identifies molecular signatures that delineate the classically defined marginal meristem / blastozone region early in leaf development. We describe and verify the importance of endoreduplication during leaf development, when and where photosynthetic competency is first achieved in the organ, regulation of auxin transport and signaling processes occurring along both the proximal-distal and medio-lateral axes, and narrow in on BLADE-ON-PETIOLE2 (BOP2) as a key regulator of margin tissue identity . CRISPR knockout mutants of BOP2 helped identify a unique phenotype of ectopic SAM formation on the complex leaf in tomato. Precise sampling practices allowed us to map gene expression signatures in specific domains of the leaf across multiple axes and evaluate the role

of each domain in conferring indeterminacy and permitting blade outgrowth. This work also provides a global gene expression atlas of the early developing compound leaf.

INTRODUCTION

A major theme in plant development is the reiteration of patterning events which are influenced by the identity and relative arrangement of neighboring plant parts. Unlike in animals, pluripotent stem cells exist throughout the entire lifetime of the plant in localized regions called meristems and generate the plant body through continued organogenesis. The Shoot Apical Meristem (SAM), which is located at the growing tip of shoots, is a dome like structure that contains reservoirs of continually self-renewing stem cells and is further defined by spatially defined zones. The peripheral zone of the SAM gives rise to most lateral organs, including leaves. The phytomer concept defines reiterated units of leaf, stem and axillary bud that make up the above ground shoot (Sussex and Kerk, 2001). Spatial organization of cells and the concept of “zones” within a plant organ have been instrumental in allowing an understanding of how cell differentiation proceeds during plant development. From molecular analyses comparing development between species, it is apparent that reiteration of developmental patterning in plants is defined by the recruitment of a common molecular toolbox, and the dizzying array of leaf architecture found on this planet is the result of variations on a common genetic regulatory program (Tsukaya, 2014; Bendahmane and Theres, 2011; Blein et al., 2008). To fully understand how leaf morphogenesis proceeds in time we spatially define the gene regulatory map of developmental domains in the tomato leaf.

Like the SAM, the angiosperm leaf has been historically defined in terms of zones and spatial cell organization. Leaf development begins from periclinal cell divisions on the periphery of the SAM and continues as cells proceed through the specific steps of development beginning with cell division, going through cell expansion, and cell specialization. In many instances this specialization involves endoreduplication. Time spent in these stages varies depending on cell position on the leaf primordium. Leaf morphogenesis and patterning occurs along three main axes - the abaxial-adaxial, proximal-distal, and medio-lateral axes. Many studies have focused on the importance of the abaxial-adaxial boundary in establishing leaf polarity (Eshed et al., 2001; Moon and Hake, 2011; Kidner and Timmermans, 2007), but for the purpose of this study we limited our focus on the relatively less studied proximal-distal and medio-lateral axes of the leaf. During development in most eudicot leaves, cells differentiate faster in the distal (top) region than in the proximal (base) region. Along the medio-lateral axis, the differentiation at the margin of a leaf is decelerated relative to the more medial regions (midvein, rachis, petiole). Thus, historically, the margin of the leaf is of particular interest because it maintains cellular

pluripotency longer and has even been argued to be a meristematic region termed the marginal meristem (Poethig and Sussex, 1985b; Avery, 1933) or marginal blastozone (Hagemann and Gleissberg, 1996a). While the developmental fate, homology, and even the name of the margin region of a leaf has been debated for around 100 years, there is general agreement that the process of cell differentiation in the margin of a leaf largely determines final leaf shape (Ori et al., 2007; Efroni et al., 2008; Scarpella and Helariutta, 2010). The regulation and modulation of margin identity on a leaf is responsible for blade expansion, serrations, lobing, vascular patterning, and new organ initiation, as in the case of leaflet initiation in compound leaves (Scarpella et al., 2010; Bilsborough et al., 2011).

Genetic regulation and coordination of leaf morphogenesis involves distinct changes in gene expression as seen from leaf transcriptomic studies in spatially defined regions across the proximal-distal axes of the simple leaved *Arabidopsis thaliana* (*A. thaliana*) (Beemster et al., 2005; Andriankaja et al., 2012; Efroni et al., 2008). These authors introduced endoreduplication, DNA replication without cell division, as a contributor to acquisition of leaf morphogenic potential (Beemster et al., 2005; Andriankaja et al., 2012; Efroni et al., 2008). The transcriptional mapping of gene expression changes in *A. thaliana* (Beemster et al., 2005; Efroni et al., 2008; Andriankaja et al., 2012), *S. lycopersicum* (tomato) (Ichihashi et al., 2014), and *Zea mays* (Maize) (Li et al., 2010) has given us an understanding of how patterning by cellular differentiation along the proximal distal axis is established, but this information is not yet precisely mapped at the transcriptome level with spatial resolution to define margin and midvein/rachis/petiole transcriptional identity.

Interestingly, one tomato mutant, *trifoliate* (*tf-2*) loses morphogenetic competence early in leaf development and is only capable of producing three leaflets - a terminal leaflet and two lateral leaflets, subtended by a long petiole (Robinson and Rick, 1954; Naz et al., 2013). The *tf-2* phenotype is caused by a nucleotide deletion resulting in a frameshift in the translated amino acid sequence of a R2R3 MYB gene (Solyc05g007870) (Naz et al., 2013). Histological and SEM analyses of the *tf-2* mutant has revealed that the marginal blastozone region is narrower, has a decrease in the number of cells, has a three-fold increase in epidermal cell size, and faster cell differentiation than the wild type background (Naz et al., 2013). While auxin application on the margin of wild-type *S. lycopersicum* leaf primordia causes leaflet initiation (Koenig et al., 2009; Naz et al., 2013), in *tf-2,* the margin is unable to make leaflets in response to exogenous auxin applications, indicating lack of organogetic competency in the margin early

in development (Naz et al., 2013). Understanding why this mutant is incapable of initiating more than two lateral leaflets, while wild type leaves continue to make on average ten leaflets at maturity (Naz et al., 2013), can help reveal the mechanisms regulating margin maintenance and identity during complex leaf development.

In this study, we used the complex tomato leaf as a system to study transcriptional mechanisms directing spatial cell differentiation processes during a key developmental stage on a young leaf, including the establishment of margin identity, proximal - distal patterning, and leaflet initiation. Since a leaf primordium develops at varying rates in a spatially defined manner, different developmental stages can be observed at the same time in a single leaf (Hagemann and Gleissberg, 1996a; Ori et al., 2007). In this study we anatomically characterize the earliest developmental stages in tomato to find the leaf age, P4, at which both the medio-lateral and proximal-distal axis are first identifiable while also containing multiple stages of leaflet organogenesis and classified the role of endoreduplication in tomato leaf morphogenetic processes. To mapped the spatial transcriptional regulation of the P4 leaf using Laser Capture Microdissection (LCM) we isolated six highly specific tissues previously unattainable in early tomato leaf development and performed RNAseq analysis to determine gene expression changes that accompany the establishment of spatial cell differentiation patterning during leaf organogenesis. We also included *tf-2* in our analysis as a comparative control, as *tf-2* lines have early loss of morphogenetic potential in the leaf margin, thus helping us uncover a cluster of genes which differ in expression only in regions that define organogenetic capacity in the margin at the P4 leaf stage. We further validate our results through molecular visualization, which provides the first evidence for when and where on a leaf photosynthesis. We also utilized CRISPR knockout lines to identify BLADE-ON-PETIOLE2 (BOP2) (Solyc10g079460) . Our approach allowed us to predict multiple verifiable gene expression differences that help explain the molecular identity of the classical described, but never transcriptionally defined marginal meristem / blastozone region and built the first global transcriptome atlas of an early developing compound leaf, which researchers can explore in the interactive Tomato EFP browser: bit.ly/2kkxsFQ .

RESULTS

Characterization of the P4 age in tomato leaf development

The goal of this work is to characterize gene expression changes that occur during tomato leaf morphogenesis. To define the scope of this our work we focused on the medio-lateral axis in an attempt to identify how the marginal blastozone maintains the potential for leaflet organogenesis and regulation of cell fate identity and further we choose to use Leaf primordium 4 (P4), the fourth oldest leaf emerging from the apical meristem (**Figure 1A and B**). P4 is a comprehensive snapshot of tomato leaflet development being composed of three distinct stages of leaflet development. The most distal region, destined to become the terminal leaflet, is undergoing early blade expansion, while the most proximal region undergoes lateral leaflet initiation, and central to these positions is the recently initiated terminal leaflet. All three regions can be anatomically defined allowing clear boundaries along both the medio-lateral and proximal-distal axes. With our scope defined, we started with a systematic survey of tissue differentiation patterns of the P4 leaf using a combination of SEM and histological approaches to establish the cellular context for detailed tissue specific gene expression analysis.

We defined the P4 leaf into three distinct regions along the proximal-distal axis, which will be hereafter referred to as top, middle, and base (**Figure 1C-G**). The top, middle, and base regions can further be split into two distinct tissues types which define the medio-lateral axis; the margin and midrib/midvein/rachis, hereafter termed rachis for clarity (**Figure 1C,G, and F**). The most distal region, the top, is the region that will ultimately become the terminal leaflet of the mature leaf (**Figure 1C**). In P4 leaves, the top margin region has already begun to develop laminal tissue (blade), has not yet developed any tertiary vasculature, but the future midvein in the top has established vascular cells including xylem and phloem (**Figure 1C**). The middle margin tissue has initiated the first lateral leaflets (henceforth called LL1), the first leaflets to form from the marginal blastozone and the rachis tissue displays clear vascular bundles and greater than four layers of cortex cells (**Figure 1F**). The most proximal area is the base, where rachis tissue has established vascular bundles (**Figure 1G**). Cells in the margin of all three regions along the proximal-distal axis are small and non-vacuolated and have likely undergone little elongation, a characteristic of marginal blastozone tissue (Hagemann and Gleissberg, 1996a) (**Figure 1C, F, and G**). Tomato leaflets initiate in pairs proximal to previous leaflet initiation sites, therefore, the next leaflets to arise, Lateral Leaflets 2 (LL2) will occur at the base

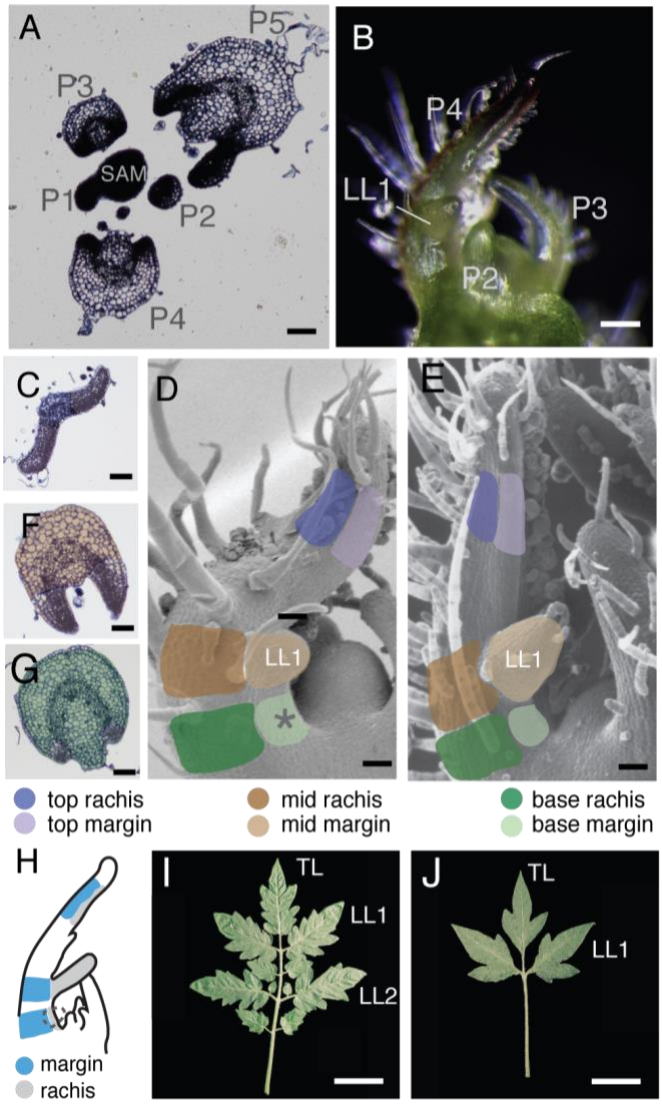

Figure 1 - Experimental set-up for sampling the *S. lycopersicum* P4 leaves
(A) Transverse section from a wild type apex showing leaf primordium P1-P5 in relation to the Shoot Apical Meristem (SAM). (B) Image of a wild type apex showing the P4 age of leaf. Images of transverse sections from the (C) top, (F) middle, and (G) base regions of a wild type P4 leaf. Colors highlight the separation of margin (lighter colors) and rachis (darker colors) along the top (purple), middle (brown), and base (green). Schematic of a P4 leaf illustrating the six identified regions in (D) wild type and (E) *tf-2*. (H) Schematic showing how this work defines margin (grey) and rachis (blue) of a leaf. Images of leaves from wild type (I) and *tf-2* (J). Scale bars (A-E) = 100 μm and (I) and (J) = 5 mm.

margin region of a P4 leaf (**Figure 1D**). To further delineate margin identity, we also characterized *tf-2*, a tomato mutant line unable to initiate leaflets past LL1, for comparison of margin identity and marginal organogenesis capacity (**Figure 1E and J**). The *tf-2* mutant diverges from wild type in developmental fate at P4, as the margin is unable to form leaflets

after LL1. Therefore, the comparison of *tf-2* and wild type allows us the opportunity to explore two leaves of comparable developmental age, but differing in organogenic potential - the ability to form leaflets. The anatomical characterization of wild type and *tf-2* shows precise cell types present across a P4 leaf, acting as a proxy for defining cell differentiation.

Cell division and endoreduplication in the P4 leaf

Conclusions made from previous transcriptomic studies tracing proximal-distal cell division patterning and cellular processing concluded that gene expression changes are responsible for the regulation of cell division, cell elongation, and endoreduplication during differentiation in developing *A. thaliana* leaves (Beemster et al., 2005; Efroni et al., 2008; Andriankaja et al., 2012; Donnelly et al., 1999). It has been suggested that endoreduplication is a defining component of *A. thaliana* leaf morphogenesis (Beemster et al., 2005; Gutierrez, 2005), with ploidy levels varying from 2C to 32C (Melaragno et al., 1993; Beemster et al., 2005). Endoreduplication occurs at the onset of leaf differentiation and elongation processes after cell proliferation, when cell ploidy levels increase due to successive rounds of DNA replication, often resulting in increased cell size (Kondorosi et al., 2000; Sugimoto-Shirasu and Roberts, 2003; De Veylder et al., 2011). While endoreduplication occurs at staggering rates (256C to 512C) during tomato fruit development (Bergervoet et al., 1996; Joubès et al., 2000; Cheniclet et al., 2005; Bourdon et al., 2010), it is currently unknown where and to what extent endoreduplication occurs during tomato leaf development. Since we could not find any work on endoreduplication in tomato leaf development, we first explicitly characterized cell division and endoreduplication processes at the P4 stage to identify similarities and differences between early leaf development in tomato and what is known in *Arabidopsis*.

To observe where cell division is occurring throughout the P4 leaf, we used 5-ethynyl-29-deoxy-uridine (EdU), which is incorporated during the S phase of the cell cycle and serves as a proxy to map cell division locations. Along the mediolateral axis, in wild type and to a lesser extent in *tf-2,* EdU fluorescence was more prominent in the margin compared to rachis tissue (**Figure 2A-F**), showing the margin tissue is actively undergoing cell division as expected in the marginal blastozone tissue. At the base margin region of wild type, where Lateral Leaflet 2 (LL2) will arise, EdU is incorporated in a cluster (**Figure 2E**), clearly demonstrating early cell division processes during LL2 initiation. Therefore, during early P4 development, although not always obvious from the external view of the leaf (**Figure 1B and D**), LL2 initiation has already begun.

The *tf-2* mutant does not show clustering of EdU fluorescence in the base margin (**Figure 2E and F**), revealing that the cell divisions needed for LL2 initiation have not occurred. In conclusion, cell division across the mediolateral axis in wild type and *tf-2* reflects similar processes occurring in *A. thaliana* (Donnelly et al., 1999) where cells are actively dividing in the margin. The cell divisions needed for LL2 initiation at P4 have already begun in wild type, but are lacking in *tf-2*, therefore mechanism that restricts LL2 initiation in *tf-2* are likely in place at the P4 stage of development.

We used flow cytometry to measure DNA content on tissue from the terminal leaflet of leaves across several developmental stages. Due to tissue limitations the youngest leaf we could test using flow cytometry of whole terminal leaflet tissue was P6 (8 days). Our results showed a combination of 2C and 4C nuclei at all ages measured (**Figure 2G**). The 4C nuclei are likely G2 nuclei after DNA replication and do not reflect endoreduplication processes, although there is a slight presence of 8C nuclei at 30 and 60 days, which might represent cell-type specific endocycling (**Figure 2G**). In *A. thaliana* plants there is a difference in ploidy levels between tip and base cells (Skirycz et al., 2011), but this was not observed in our data (**Figure 4H**). We conclude that endoreduplication is not as pronounced in tomato as in *Arabidopsis*, and likely not a vital aspect of tomato leaf morphogenesis, illustrating the diversity of cellular in processing in leaf morphogenetic strategies between species.

Laser capture of six regions of the P4 tomato leaf

Since the P4 leaf is representative of many key developmental processes that define leaf development: 1. margin vs rachis specification and 2. leaflet initiation and morphogenesis, we analyzed the P4 stage more explicitly. We took advantage of our comprehensive anatomical characterizations to provide a map which delineates the medio-lateral axis and leaflet organogenesis. We employed Laser Capture Microdissection (LCM) following explicit rules for tissue collection (**S1 Figure**) on P4 leaves of both wild type and *tf-2* lines to capture gene

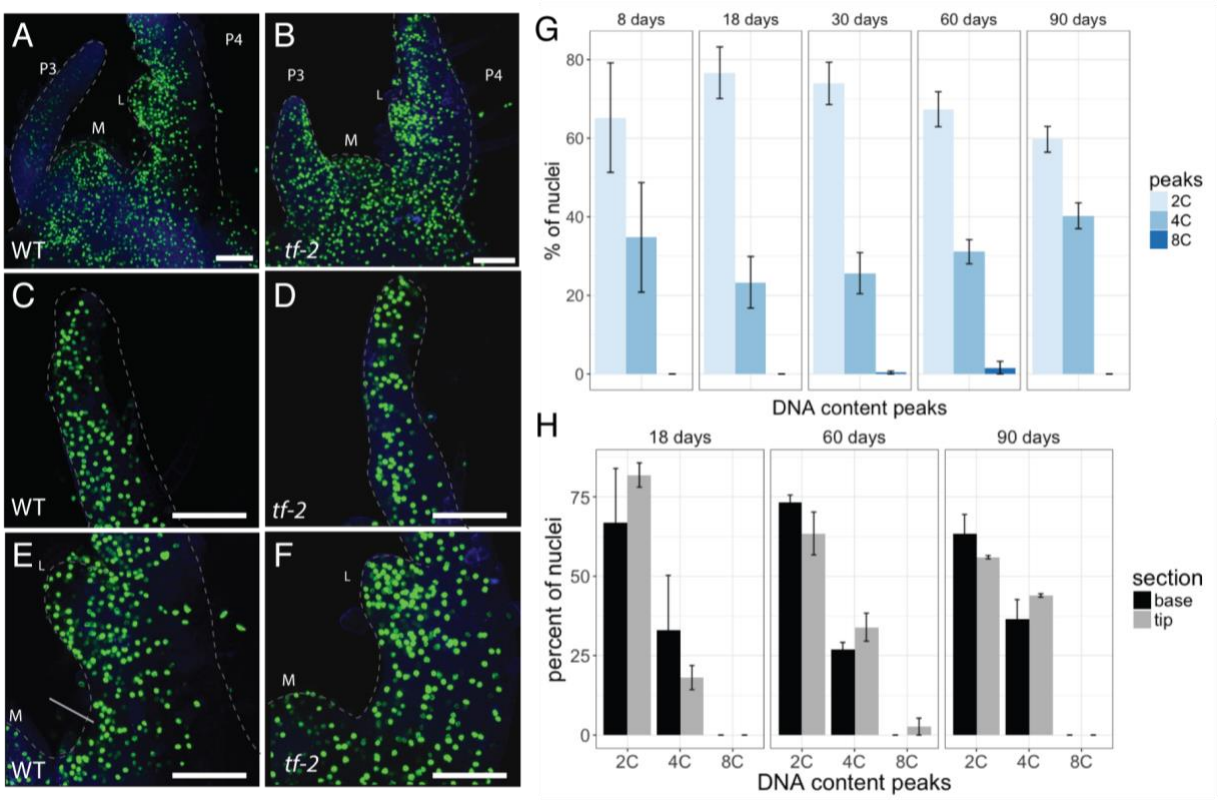

Figure 2 - Cell cycle characterization using Edu Fluorescence and Flow Cytometry
(A-F) Representative confocal images using EdU fluorescence to detect sites of cell division at the shoot apex of (A,C,E) wild type and (B,D,F) *tf-2* plants. Images showing the (C-D) top region of a P4 leaf, while (E-F) shows middle and base regions of a P4 leaf. Arrow in (E) points to clustering of EdU fluorescence suggesting sites of active cell division needed for leaflet initiation. (G) Bar graph showing DNA content peaks from flow cytometry on leaf tissue. Tissue was collected from Leaf 5 from plants grown 8-90 days after germination. (H) Bar graph displaying the DNA content peaks from flow cytometry comparing leaf tissue sampled from the base (black) to tip (grey). Error bars show the standard deviation across at least three replicates at each time point. Scale bars = 100 μm.

expression differences that might explain the morphogenetic differences in the margin of *tf-2* plants. Tomato apices were sectioned transversely to isolate the same six sub-regions in both wild type and *tf-2*, (1) top margin blastozone region (top margin), (2) top rachis, (3) middle margin, (4) middle rachis (5) base margin, and (6) base rachis (**Figure 1C-G, Movie 1**). We attempted to collect enough tissue for seven replicates per sample, but due to the fragility of RNA at such a small tissue size, a few replicates did not pass quality control and were lost at various steps in the pipeline, resulting in a total of 3 - 6 biological replicates per region (**Figure 3A**). We collected tissue from 6-8 apices per biological replicate to achieve a minimum of 2ng of RNA per replicate. The number of cuts needed to achieve minimum RNA amount varied depending on sample and tissue density and total tissue area collected also varied between

samples (**S2 Figure A - C**)**.** The isolated mRNA from collected tissue was further amplified and prepared for Illumina sequencing (see Materials and Methods).

Each replicate resulted in an average of 4.9 million sequencing reads (**Figure 3A**). To assess overall similarity between samples, gene expression values were visualized in Principal Component (PC) space for each of the six subregions per genotype. In wild type there is a clear separation of margin and rachis regions, as like samples cluster together in PC space (**Figure 3B**). In *tf-2* samples, the margin and rachis regions are not as distinctly differentiated (**Figure 3B**), suggesting similarity in cell type identity between margin and rachis at the top region of P4 due to early loss of meristematic potential in the marginal blastozone region of the *tf2* primordium (Naz et al., 2013).

Differential gene expression between wild type margin and rachis tissue along the proximal-distal axis reveals signatures of morphogenetic states during early leaf development

To gain a specific understanding of the differences between margin and rachis tissue in the three regions along the proximal-distal axis we performed pairwise differential gene expression on wild type samples comparing margin and rachis in each region (top, middle, base) (**Dataset S1**). Genes that are differentially regulated in margin versus rachis in each region will describe gene expression patterning along the medio-lateral axis. We performed differential gene expression between margin and rachis in the top, middle and base regions separately using edgeR (Robinson et al., 2010) (see Materials and Methods). Gene Ontology (GO) enrichment

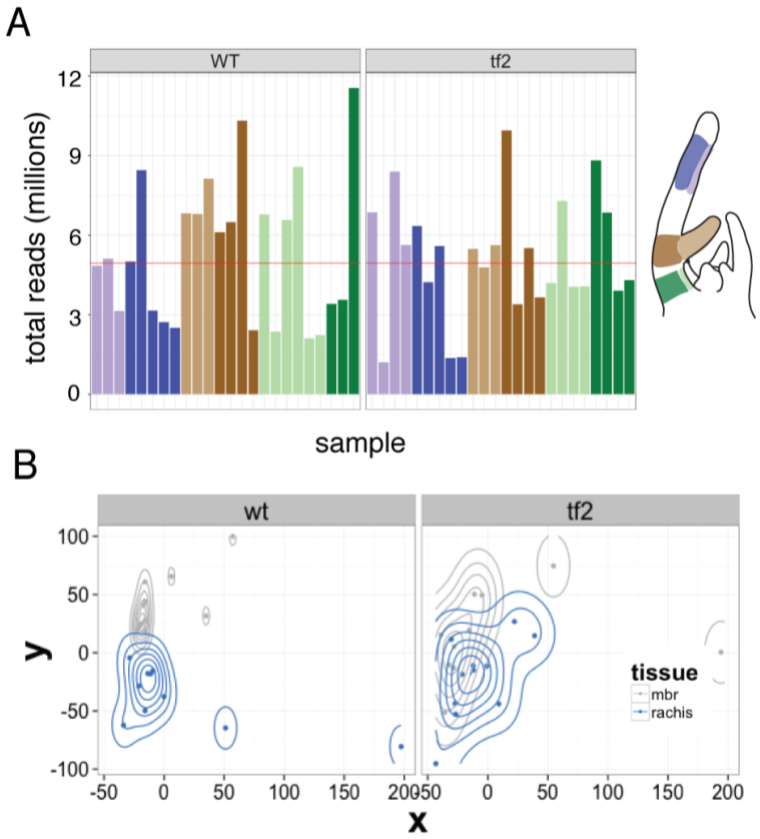

Figure 3 - mRNA from laser capture microdissection (LCM) and summary of read results from Illumina sequencing
(A) Boxplot illustrating total reads mapped to the *S. lycopersicum* genome per replicate in each sample region. Red line indicates mean across all samples. (B) Principal component analysis of gene expression pattern of normalized reads from margin (grey) and rachis (blue) tissue.

was determined for the genes that are significantly up-regulated (BH-adjusted p value < 0.05) (**Dataset S2**). When comparing the margin and rachis tissue, the margin region, which has historically been considered to proceed at a slower rate through the morphogenetic stages, has up-regulation of more GO terms associated with cell processes occurring early in morphogenesis. For example, when we test for genes that are significantly differentially expressed between the margin and rachis tissue in the top region, we see 603 genes that are up-regulated in the margin (**Figure S3**) and are GO enriched with terms likely reflecting cell division processes occurring including chromatin and DNA processing (**Figure 4A, Dataset S2**). Conversely, genes up-regulated in the rachis are significantly enriched in GO terms reflecting the cell specialization stage of morphogenesis, and include transport, photosynthesis, sugar biosynthesis, \and carbohydrate metabolism (**Figure 4A-C, Dataset S2**). When we compare margin and rachis in the most proximal region, the base, we see DE of up-regulated of 1722

genes which show enrichment for GO categories related to cell division, chromatin assembly, and DNA processing in the rachis, and only 94 DE down-regulated genes in the margin region at the base (**S3 Figure A**), showing enrichment for the GO term related to transcription factor activity and auxin influx (**Figure 4A, Dataset S2**). The types of genes differentially expressed between the margin and rachis also appear to reflect which stage of morphogenesis the region is in and may demonstrate the distal to proximal wave of differentiation (**Figure 4B and C**). The up-regulated genes in the top and middle margin regions are enriched in GO terms describing active RNA, DNA, and chromatin processing, but in the base up-regulation of similar GO categories is seen in the rachis. The active processing of RNA, DNA, and chromatin, are key gene expression signatures of cell division and expansion, and the base region of the P4 leaf is still in these middle stages of morphogenesis and just beginning to start secondary cell wall biosynthesis and specialization in sucrose transport activity (**Figure 4A, Dataset S2**).

Taken together, differential gene expression analysis encapsulated in the GO terms describing different stages of morphogenesis indicates two trajectories of development along the leaf, 1. along the proximal-distal and 2. along the medio-lateral axis (**Figure 4B and C**). Cells that have achieved specialized photosynthetic function, leaf development, and sugar transport define the final morphogenetic stages. Margin regions undergoing active cell division are defined by chromatin assembly and DNA processing (replication, integration and recombination) required for proper cell cycle progression, while the most meristematic tissue in the margin region at the base, is defined by only transcription activity and TF and DNA binding (**Figure 4A-C**). Thus the P4 tomato leaf represents a complex mix of developmentally distinct regions that cannot be defined solely along the proximal-distal or medio-lateral axes.

Modeling gene expression differences across the medio-lateral axis predicts photosynthetic activity occurring first in the rachis

Performing differential gene expression analysis in each region along the proximal-distal axis reveals specific genes and GO categories that are unique to either the top, middle, or base, but we wanted to ask if there is gene activity that defines rachis and margin identity across the

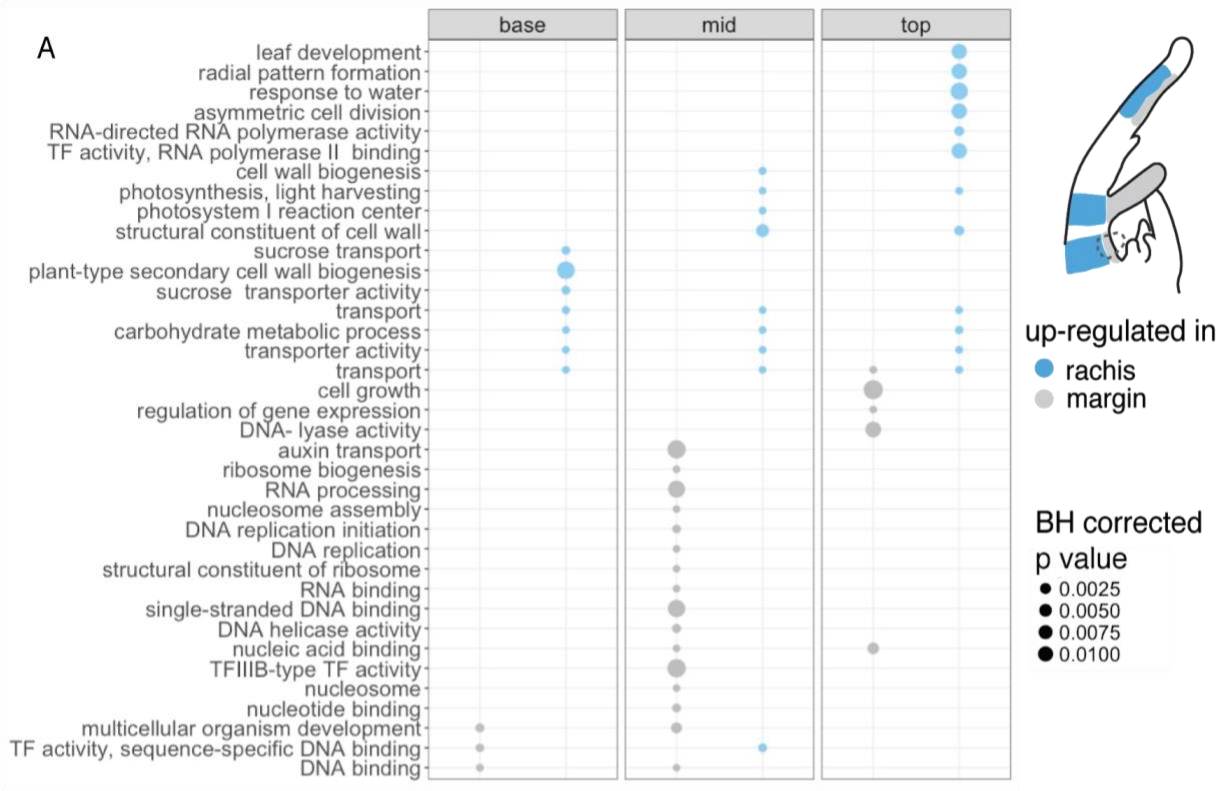

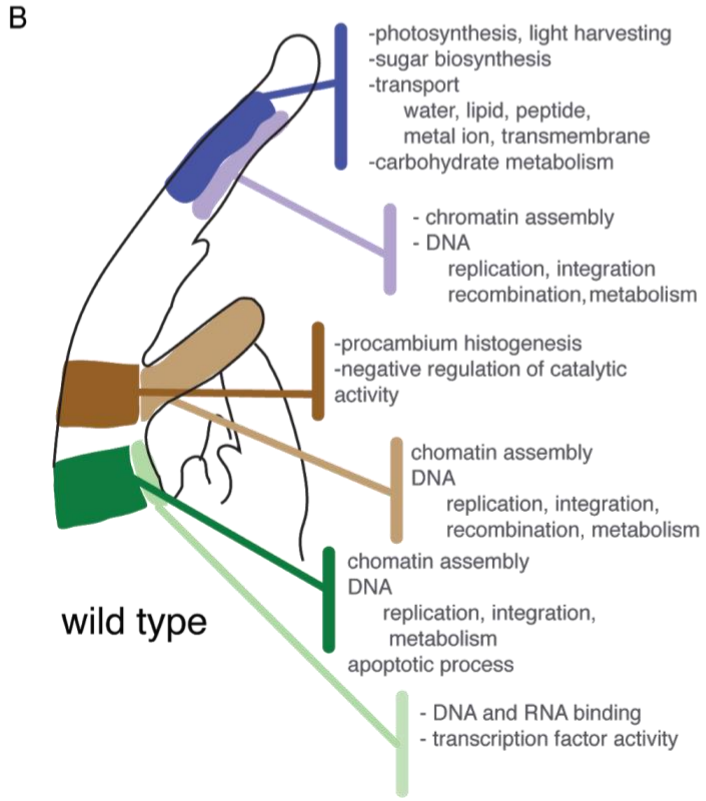

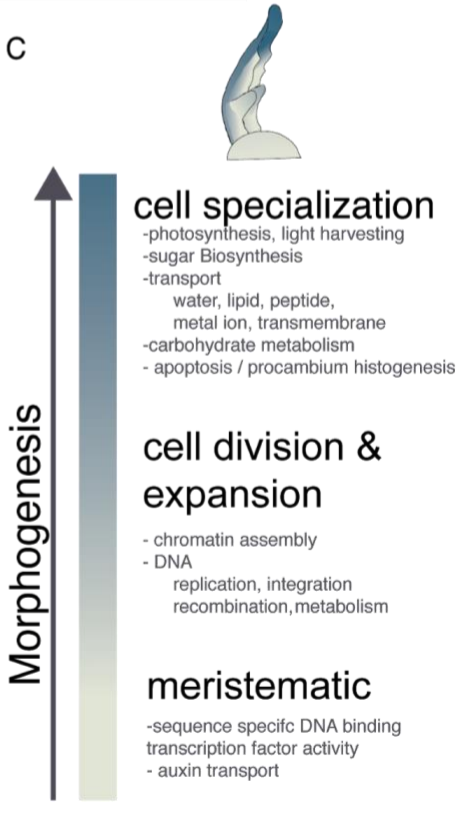

340

Figure 4 - Pairwise differential gene expression between rachis and margin in each region along the proximal-distal axis in wild type P4 leaf
(A) Graph summarizing representative GO terms enriched describing the significantly up-regulated genes in each region (top, mid, and base) from differential gene expression analyses performed on wild type plants. Point size represents Benjamini-Hochberg (BH) corrected P-values in margin (grey) and rachis (blue) tissue. (B) Schematic summarizing GO enriched terms observed from differentially up-regulated genes in each region of the P4 leaf. (C) Schematic encapsulating GO categories that help define each morphogenetic state along the leaf.

entire P4 leaf primordium regardless of position in the longitudinal axis. To answer this question we performed differential gene expression across the margin and rachis tissue and to adjust for variability between the proximal-distal axis, we employed an additive linear model using the top, middle, and base identities as a blocking factor in our experimental design using EdgeR (Robinson et al., 2010). In wild type, across the entire proximal-distal axis, we found 1,089 genes that were significantly up-regulated in rachis and 188 genes that were significantly up-regulated in the margin (**Figure 5A, Dataset S3**). We proceeded with GO enrichment to describe the differentially expressed genes and found 24 GO terms enriched in the genes up-regulated in the rachis (**Dataset S4**). Summarizing these terms, we identified eight main categories; Sugar Biosynthesis and transport, Metabolism (carbohydrate and glucose), Photosynthesis / light harvesting, Response to light, Transmembrane transport, and Catalytic Activity, protein phosphorylation / kinase activity (**Figure 5B**) which characterize genes that are up-regulated in the rachis compared to the margin across the entire proximal-distal axis. These results suggest the rachis region of a P4 leaf has many specialized tissue types and may already be physiologically active.

Verifying photosynthetic gene expression patterns

Of the gene expression patterns discovered above, the most prominent pattern found when performing both pairwise and modelled DE analyses was the persistent presence of genes associated with GO terms related to photosynthetic processes, and these genes were up-regulated in the rachis compared to margin tissues (**Figure 4 and 5**). While up-regulation of genes involved in cell wall development, leaf development, and transport might be expected in the rachis, a region of the leaf that acts as a connective corridor to the rest of the plant, we were surprised to find up-regulation of so many genes defined by GO categories involved in photosynthesis. As noted in the previous pairwise differential expression analysis, the most

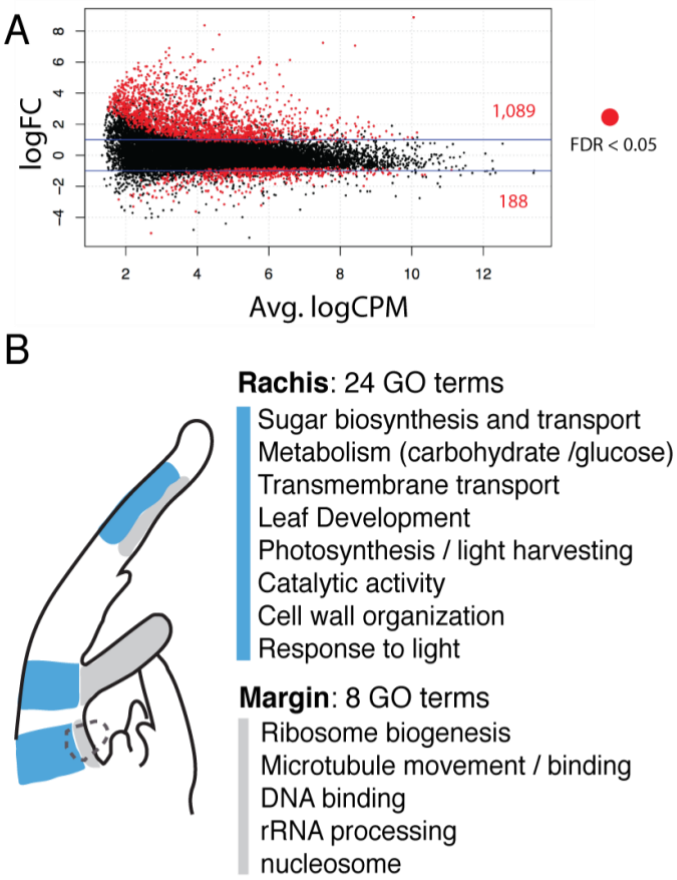

Figure 5 - Differential gene expression modelled between margin and rachis in wild type P4 leaf (A) Results from differential gene expression in wild type displaying average log Counts Per Million (LogCPM) over log Fold Change (logFC), illustrating the number of significantly differentially regulated genes (red) between margin and rachis tissue. (B) Summary of GO terms describing up-regulated genes in each tissue, showing the rachis (blue) tissue is predominantly described by GO terms related to cell specialization compared to margin (grey).

abundant GO enriched categories for up-regulated gene activity in the rachis are those related to sugar biosynthesis and photosynthesis, indicating that the rachis region likely has functioning photosynthetic machinery prior to the P4 margin, which is destined to become the primary photosynthetic tissue of the leaf - the blade. Since little is known about when photosynthesis first begins in a developing leaf and we could find no previous studies describing photosynthesis specifically in the rachis, we wanted to verify our gene expression results which suggest the rachis as a photosynthetic force early in leaf development.

To verify the photosynthetic signature repeatedly found up-regulated in rachis compared to margin tissue we searched for photosynthetic genes in our dataset that showed significant differential gene expression between the rachis and margin in each of the longitudinal regions. We identified three *Light Harvesting Chlorophyll A-B binding genes* (*CAB*) genes (Solyc03g005760 (*SlCAB1*), Solyc03g005760 (*SlCAB2*), Solyc03g005760 (*SlCAB3*) which had significantly up-regulated expression in the rachis regions compared to margin (**Figure 6A**, **Data S1**). CAB proteins act as a mechanism for balancing excitation energy between Photosystem I and II during photosynthesis (Liu and Shen, 2004) and are an important component of photosynthesis.

In an attempt to 1. verify the gene expression differences identified in our experimental set-up, and 2. visualize when and where a leaf primordium begins photosynthetic activity, we made a transgenic line expressing a representative CAB gene promoter attached to the β-glucuronidase (GUS) reporter to aid in visual localization (pCAB1::CAB1::GUS) (Mitra et al., 2009; Tindamanyire et al., 2013). We found that in the expanded leaflets of P9 leaves, pCAB::CAB1::GUS expression is nearly ubiquitous across the entire blade (**Figure 6B**) and at this age the leaf has the anatomy of a fully functional photosynthetic organ. As predicted from our differentiation gene expression analysis, we found a clear pCAB::CAB1::GUS signal localized predominantly in the rachis region along the proximal-distal axis in younger leaf primordia (**Figure 6C**). The pCAB::CAB1::GUS signal spreads to the distal tips of newly established leaflets and lobes early in development, and then continues to spread along the margin region as the leaf continues to develop, until the entire leaf shows expression (**Figure 5B-D**). Since pCAB::GUS is predominantly expressed in the rachis region early in development, we suggest that the rachis is the first photosynthetic region in a developing leaf to function photosynthetically as predicted in our RNAseq analysis. Previous studies have hinted at chloroplast retrograde signaling and sugar functioning to trigger leaf differentiation processes (Andriankaja et al., 2012; Lastdrager et al., 2014). In the light of these studies, the enrichment of photosynthetic genes seen in the rachis provides the first evidence that the rachis region of very early developmental stage, P4, is not just functioning as a conduit for nutrients and water transport, but also photosynthesis and sugar production. Considering the suggestion that photosynthetic activity and sucrose and may help direct regulation as signalling molecules of cell differentiation and leaf morphology (Lastdrager et al., 2014; Wind et al., 2010), we

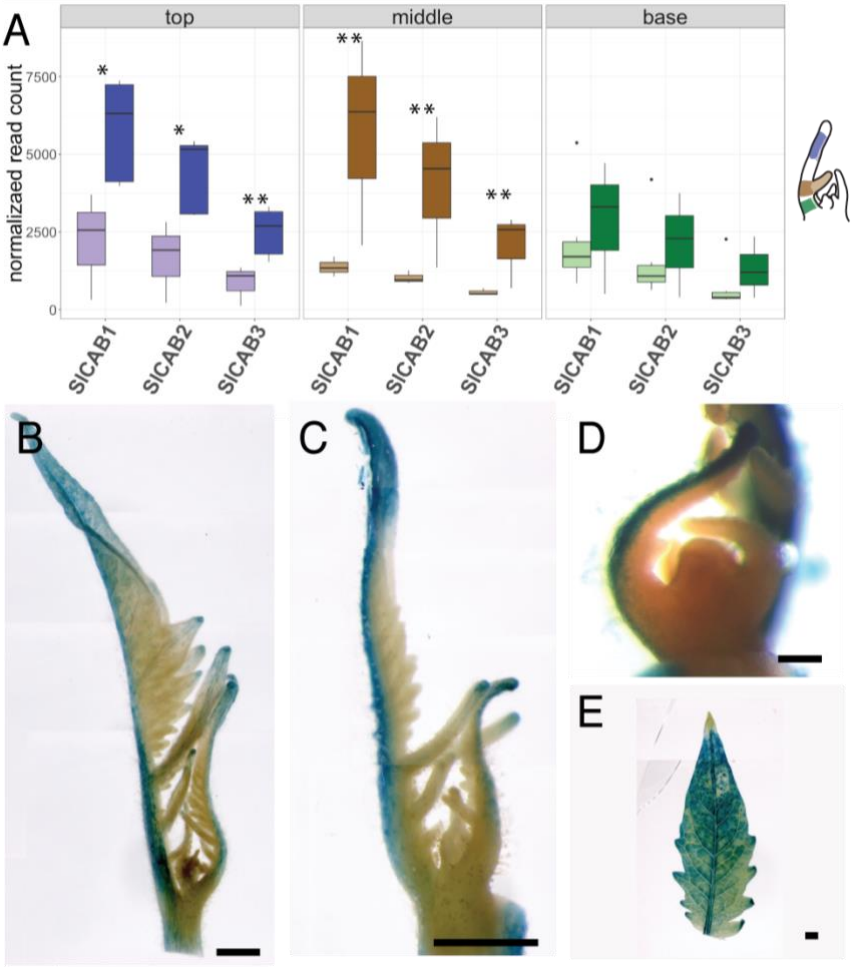

Figure 6 - Chlorophyll A-B binding gene activity is up-regulated in rachis compared to margin tissue during early leaf development

(A) Normalized read count for Chlorophyll A-B (CAB) binding genes in tomato (SlCAB). (B-E) pCAB::GUS expression showing photosynthetic activity during leaf development in tomato. pCAB::GUS is localized in the rachis of P4-P6 leaflets, illustrating differential regulation of CAB along the medio-lateral axis during early leaf development. pCAB::GUS is nearly ubiquitous in (E) P8 terminal leaflet. * p-value < .005 of significantly up-regulated in the rachis tissue compared to margin from modelled differential expression analysis. Scale bars (B-C, E) = 1mm, (D) = 100 µm.

hypothesize a potential functional role for the rachis region during early leaf morphogenesis - as a signaling center for cell differentiation.

Self Organizing Maps identify explicit groups of genes that share similar expression patterns

In order to refine our results and determine if there are groups of genes that share similar co-expression patterns that may be too complex to define by DE analysis alone, we used Self

Organizing Mapping (SOM) to cluster genes based on gene expression patterns across the six tissue groups. SOM (Tamayo et al., 1999) begins by randomly assigning a gene to a cluster, then genes are subsequently assigned to clusters based on similar gene expression in a reiterative process informed by previous cluster assignments. This clustering method allows genes to be grouped based on specific gene expression patterns shared across different tissues, allowing classification into smaller gene groups not possible by DE analysis alone. In addition, SOM analysis also provided a means to survey the most prominent types of gene expression patterns found in our data.

To focus on the most variable genes across tissue we used the top 25% of genes based on coefficient of variation, resulting in a dataset of 6,582 unique genes (**Dataset S5**). We first used principal component analysis to visualize groups of genes and found the first four principal components explained 31.9%, 26.2%, 19.0%, and 13.5% of the amount of variation in the dataset respectively (**S5 Figure A**). Looking at the expression of these genes in PC space, distinct clusters of genes with related expression patterns are revealed (**Figure 7A**). To find the most common gene expression patterns that describe the data, SOM analysis was first limited to six clusters (**Dataset S6**). One of the six clusters, Cluster 4 with 1090 genes, defines a clear separation of margin and rachis tissues, which again reinforces the previously found trend that many genes have a difference of expression depending on where they are localized along the medio-lateral axis (margin vs rachis). This cluster is enriched in genes defined by Carbohydrate metabolic processes, hydrolase activity, protein dimerization, membrane, transporter activity, and photosynthesis and light harvesting (**S5 Figure, Dataset** S7). This analysis mirrors the results obtained from the Differential gene expression analysis and reflects the overall abundance and diversity of genes up-regulated in the rachis which comprises the largest signal in our dataset, likely reflecting the specialization in tissue occurring as the rachis develops an identity distinct from margin.

Auxin transport and regulation as a defining feature of margin identity

In order to refine our questions of gene expression patterns to just those that direct margin identity, we specified a larger clustering map. We used this approach to obtain a smaller subset

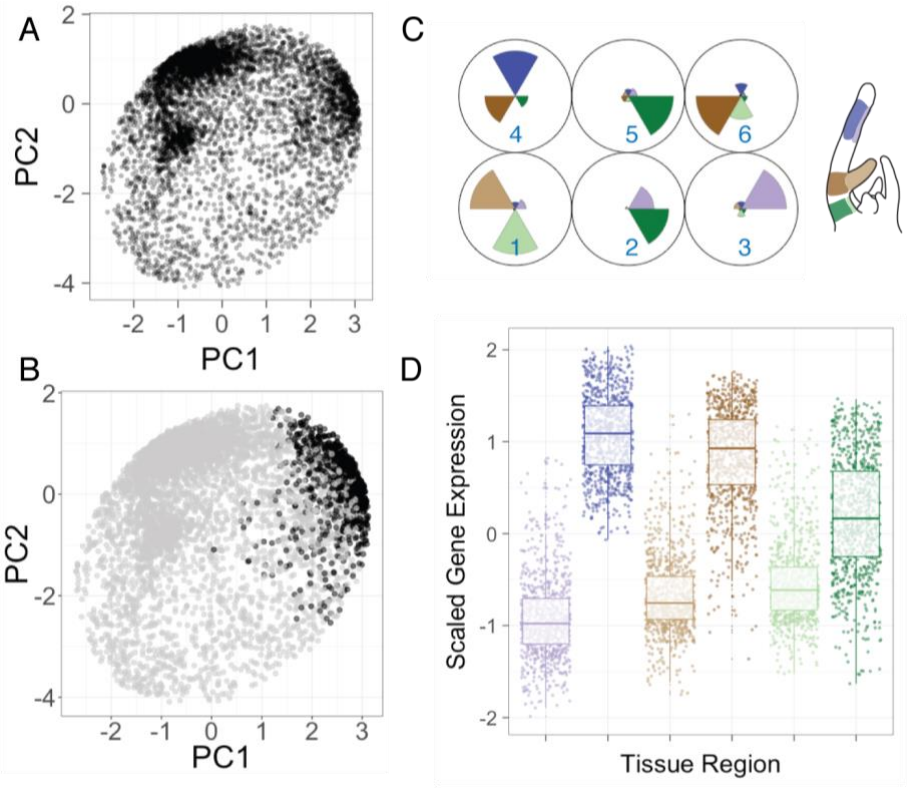

Figure 7 - Top clusters resulting from SOM analysis define each tissue region by up-regulated genes

(A) Plotting of wild type gene expression observed in the top 25% of genes based on coefficient of variation in Principal Component (PC) space. (B) Projection of SOM cluster 4 onto PC space explains one of the main clusters in PC space (C) Codebook vector of a 2x3 SOM analysis showing the top six clusters (D) Gene expression pattern of Cluster 4 across the six tissue types.

of genes than was possible in differential gene expression analysis, or SOM clustering using a smaller number of clusters. We were especially interested in specific types of gene expression patterns that defined the medio-lateral axis and in this case, we looked for groups of genes that are preferentially up or down-regulated in the margin compared to the rachis. We specified 36 clusters in a 6x6 hexagonal topology forcing interactions between multiple tissue types (**Figure 8A, S6 Figure**). We surveyed the gene expression patterns of each of the 36 clusters (**Dataset S8**) and identified clusters 10 (n =108) and cluster 11 (n=112) that describe a group of genes which are up-regulated in the margin and down-regulated in the rachis tissues types in the P4 wild type plants (**Figure 8B - C**). While over half of these genes (57.2% - 126 / 220) had no known function, of the remaining genes, many were genes known to be involved in leaf margin identity (**Table 1**). Interestingly, clusters 10 and 11 also contained genes related to auxin transport and biosynthesis, and regulation (YUC4, PIN1, AUX2-11) and genes known to

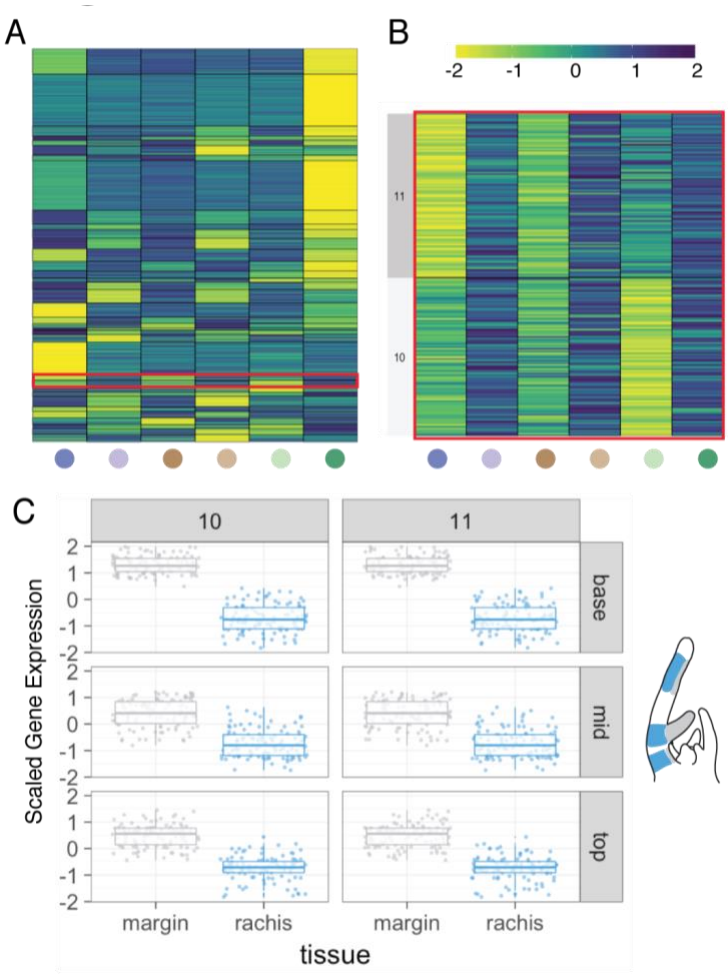

Figure 8 - Large SOM map describes a small gene cluster which defines margin identity
(A) Heatmap representing the gene expression pattern of the 36 clusters of genes (red) box highlights clusters 10 and 11 (B) Heatmap of specifically clusters 10 and 11 which have a gene expression pattern of genes which are up-regualted in the margin, while down-regulated in rachis. (B) Boxplot showing the gene expression pattern of cluster 10 and 11.

regulate auxin (ARGONAUTE). Guided by the gene expression characterization in wild type, we wanted to see how gene expression is different in *tf-2* which could explain the striking feature of loss of meristematic potential in the basal margin of *tf-2.*

We then wanted to look explicitly at the differences in auxin transport present between *tf-2* and wild type. To verify the *SlPIN1* gene expression differences found between wild type and *tf-2,* we crossed a fluorescently labeled pPIN1::PIN1::GFP line (PIN1::GFP) (Benková et al., 2003; Koenig et al., 2009) with *tf-2* to visualize differences in PIN1 localization and expression in P4 leaves. In wild type, PIN1::GFP is present along the entire margin region of a P4 leaf, with highest signal present at the site of the newly established LL1 (**Figure 9A and B**). In *tf-2,* there

is an overall decrease in fluorescence signal along the margin of a P4 leaf. Also, *tf-2* has a noticeable decrease in PIN1::GFP fluorescent signal in the base margin region (**Figure 9C and D**). In addition, we visualized auxin presence with the use of auxin inducible promoter DR5::Venus (Bayer et al., 2009) . As observed previously in wild type (Shani et al., 2010; Martinez et al., 2016), DR5::Venus is expressed at the site of leaflet initiation as a sharp wedge shaped focus region (**Figure 9E - F**). By contrast, in *tf-2* there is an auxin focus, but it is diffuse and located in the upper layers of the margin (**Figure 9G-H**). These results support the hypothesis that *tf-2* is capable of making auxin foci, it is incapable of maintaining proper auxin foci and canalization processes as evidenced by the reduction of PIN1 expression in the basal margin region of the *tf-2* P4 leaf. The transcriptomic results and auxin visualization experiments suggest auxin transport and biosynthese, and specifically *SlPIN1* misregulation, are important contributors to the *tf-2* phenotype and vital regulators of margin organogenesis.

Gene expression patterns differences between wildtype and *tf-2* help define meristematic loss in *tf-2*

We included *tf-2* in this study because of the intriguing phenotype of losing the ability to make new leaflets after the first two LL1 leaflets in this mutant. At the P4 stage *tf-2* has already lost the organogenetic ability to initiate new leaflets. We know from our auxin transport visualization analysis that *tf-2* appears to receive a leaflet initiation signal, as it is capable of forming auxin foci (**Figure 9H**), but the tissue is unable to initiate leaflet organs. We looked to our data to characterize if there are gene expression differences that could explain the loss of meristematic competency in *tf-2*. Differential gene expression analysis was performed with only *tf-2* reads and the first observation was that there were a lot fewer differentially expressed genes between margin and rachis in each of the top mid and base regions (**S3 Figure A, Dataset S1**). We saw that indeed *tf-2* followed similar gene expression trends when margin and rachis identity were compared. The margin was more enriched in genes related to cell division and cell expansion, while the rachis was enriched in genes with GO terms related to specialization including water transport, metabolic processes, photosynthesis, leaf development; however, these distinct differences were mostly apparent in the base region of the *tf-2* mutant (**S4 Figure B**). The main differences between wild type and the *tf-2* mutant were a reduction in up-regulated differentially expressed genes in the rachis region compared to margin in top, mid, and base (**S3 Figure A**).

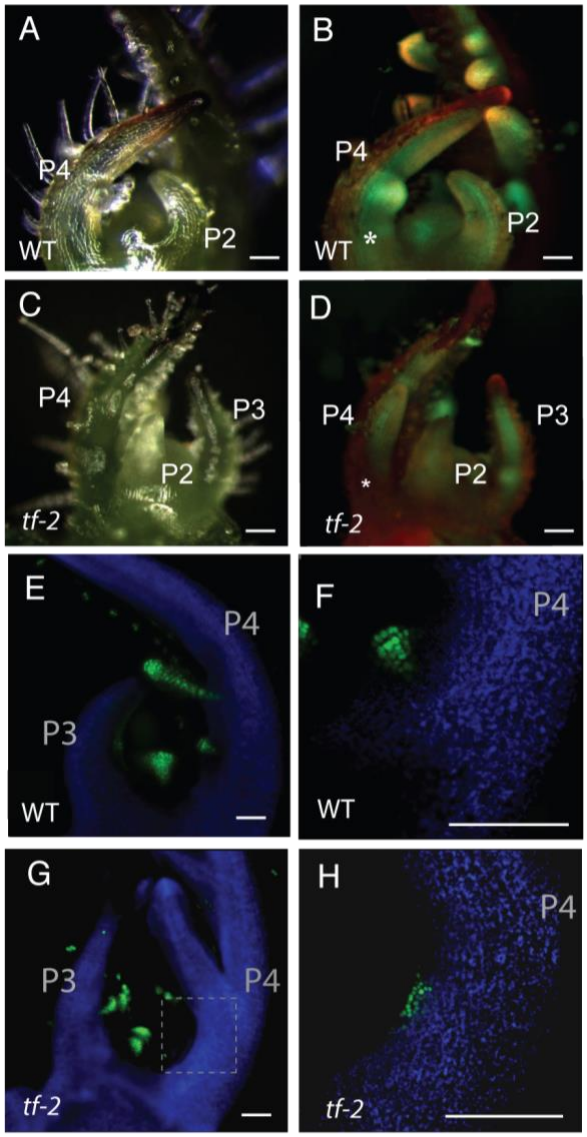

Figure 9 - Auxin visualization during leaflet initiation in wild type and *tf-2*

(A)-(D) Microscope images of apices from (A) and (B) wild type and (C) and (D) *tf-2* . (B) and (D) Fluorescence signal of PIN1::GFP (green) and chlorophyll autofluorescence (red). (B) shows clear PIN1::GFP signal in wild type along the entire margin of the P4 leaf, while in (D) *tf-2* has lost signal in the base marginal blastozone region. (E)-(H) DR5::Venus signal using confocal. Scale bars = 100 μm.

It should be noted that while wild type and *tf-2* are the same morphologically, the *tf-2* mutant does appear to be further along in morphogenesis process at all regions (top, middle and base), a featurep described by Naz and coworkers (2013). This overall difference in the two genotypes should be taken into account at both the morphological, and as evidenced by this transcriptional analysis, molecular levels. In the margin of *tf-2* we looked at which genes are DE between the rachis and margin and found many genes related to leaf development.

Taking into account the general overall differences between these two genotypes, we were still interested in understanding why *tf-2* is unable to initiate lateral leaflets beyond LL1. Are there transcriptional differences that could explain the loss of morphogenic capacity in *tf-2*? Is the difference observed between wild type and *tf-2* purely a morphological time point difference or is it because of differential gene expression? In order to ask these questions, we combined both genotypes and used a generalized linear model (glmQLFTest in edgeR) where we defined each genotype as a group and therefore could make contrasts between the two genotypes at each of the top, middle, and base regions. When we compared the base margin region between *tf-2* and wild type (**Figure 1A**), there were only 23 genes that were differentially expressed and all of them were downregulated in wild type compared to *tf-2* (**Table 3**). We focused on the twelve genes that were functionally annotated, and noticed *Blade-On-Petiole* (*SlBOP2*) was found significantly up-regulated in the margin of *trifoliate* compared to wild type (**Figure 10B**).

We then explored the function of *SlBOP2* in regulating margin and rachis tissue identity by phenotyping CRISPR/Cas9 gene edited loss-of-function *SlBOP2* mutations (*CR-slbop2)* (Xu et al., 2016). We focused on leaf phenotypes and surprisingly in the *CR-slbop2* plants, we observed ectopic meristems along the adaxial rachis of the mature leaves at the base of primary leaflets (**Figure 10C, D, E**). The BOP2 ectopic SAM structures did not persist into maturity, and only on rare occasions generate complex leaf-like organs (**S7 Figure**). Loss of *SlBOP2* function also resulted in increased leaf complexity (**S7 Figure**) as previously reported (Xu et al., 2016) and *SlBOP2* knockdown lines (Ichihashi et al., 2014). Since TF is a known transcription factor, we checked for TF binding site motifs in the 3KB upstream region of BOP2 and found one TF binding site (**Figure 10F**). Taken together *SlBOP2* functions in margin meristematic identity along the rachis of the leaf, possibly through direct binding interaction with TF to the upstream regulatory region of SlBOP2

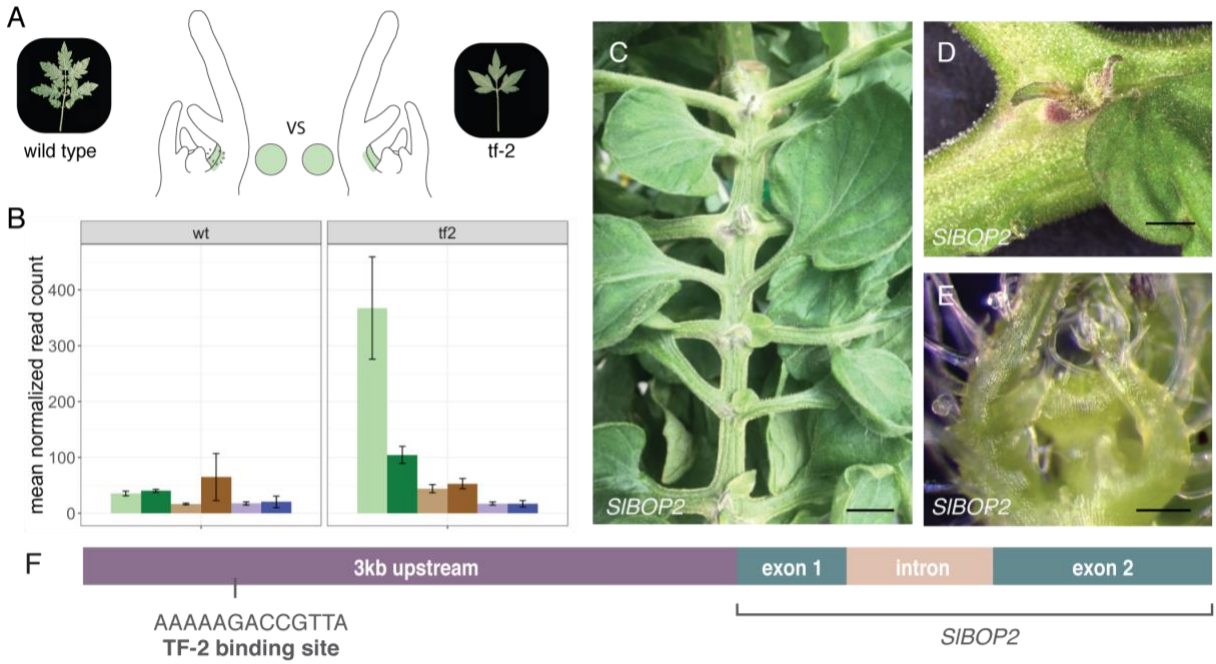

Figure 10 - Differential gene expression in base margin tissue between wild type and *tf-2* reveals BOP2 as a regulator for suppression of meristematic identity

(A) Schematic illustrating the regions (base margin) which were compared between wild type and *tf-2* using modelled differential gene expression analysis (B) Bar graph illustrating the gene expression of *SlBOP2* across all six tissue types between wild type and *tf-2,* showing how *SlBOP2* is upregulated in the base margin in only the *tf-2* line. (C) - (E) *SlBOP2* CRISPR knockout line (*CR-slbop2*) which displays ectopic shoot apical meristems along the rachis of complex leaves (F) *SlBOP2* genomic region, black line demarcates location on *TF-2* binding 3kb upstream of *SlBOP2*. Scale bars (C) = 10mm, (D) = 2 mm, (E) = .2mm

DISCUSSION

Unique genetic signatures define leaf development along the proximal distal and medio - lateral axes

The overall goal of this work was to use gene expression signatures to gain a better understanding of the processes that regulate morphogenesis along the rarely explored medio-lateral axis in an early developing compound leaf. Anatomical analysis informed the choice of six unique regions in the P4 leaf (**Figure 1C-F**). We analyzed differential gene expression between margin and rachis tissue in each of the top, middle, and base regions, identifying signature patterns of gene regulation along the proximal - distal (tip - base) axis (**Figure 4**) that help define leaf morphogenesis in the early tomato leaf primordium.

In addition to a basipetal wave of differentiation along the proximal-distal axis, the leaf differentiates from the midrib/rachis out into the margins at each region on the proximo-distal axis. These two regions, the margin and rachis, have distinct developmental trajectories; the rachis matures early and the marginal blastozone retains some meristematic potential and gives rise to the leaf blade region as well as leaflets in compound leaves. Separating the rachis from the marginal blastozone region at three different points along the proximal-distal axis allowed us to determine whether development proceeds uniformly along the proximal-distal axis or if the leaf has a mosaic of developmental states in each segment along the proximal-distal axis. The further along in morphogenesis a region was, the more diverse GO categories of genes were up-regulated in the region, likely reflecting the last stage of leaf morphogenesis, cell specialization, has occurred. After summarizing the GO terms enriched in each of the three regions along the proximal-distal axis, clear patterns of developmentally distinct processes were identified in the rachis regions compared to other tissues (**Figure 4**). The margin regions, classically defined as the marginal blastozone or marginal meristem, retain the potential to divide and differentiate but also in a basipetal gradient. Thus defining leaf development or capturing gene expression in entire primordia, or even in regions along the proximal-distal axis does not give an accurate picture of developmental patterns in a leaf. Further dissection of events at cellular resolution will define these patterns even better.

Photosynthetic capability in the rachis as a regulator of medio-lateral differentiation

To further define rachis and margin identity we fitted an additive model which adjusts differential expression comparisons based on baseline differences that occur between margin and rachis. We then proceeded with differential gene expression analysis, essentially revealing gene expression trends which define margin and rachis tissue, regardless of position on the proximal-distal axis. The most prevalent, though unexpected, gene expression signature we observed was the enrichment of genes associated with photosynthesis in the rachis which we found in both our DE analysis (**Figure 4 and 5**) and in our cluster analysis (**Figure 7**). Since little is known about when photosynthetic capacity is acquired during early leaf morphogenesis, we further verified photosynthesis activity using a CAB::GUS reporter (**Figure 6**). This work suggests photosynthetic activity is acquired as early as the P4 and is not uniformly distributed along the proximal-distal and medio-lateral axes. When viewed in the context of cell differentiation processes along each axis, it is intuitive that specialized functions are acquired first in regions that mature earliest, but the function of photosynthesis has been traditionally

assigned to the blade. What are the developmental consequences of sugar biosynthesis in the rachis during early leaf organogenesis? Could the rachis be the source of morphogenic signaling towards the more immature base along the proximal-distal axis and along the medio-lateral axis to the margin? Multiple studies in *A. thaliana* show thousands of genes respond to changes in sugar levels by modification of transcript abundance (Price et al., 2004; Bläsing et al., 2005; Osuna et al., 2007; Usadel et al., 2008). In light of our understanding that the main photosynthetic product, sugar, is a known signal for plant development and growth. In the P4 primordium under study, while the rachis has acquired specialized functions, the margin is actively dividing, a process reliant on cell cycle progression. Critical regulators of the cell cycle, cyclins CYCD2 and CYCD3, are up-regulated in response to sugar (Riou-Khamlichi et al., 2000). Interestingly, sucrose has also been shown to influence auxin levels (Lilley et al., 2012; Sairanen et al., 2012), transport and signal transduction (Stokes et al., 2013), and metabolism (Ljung, 2013). Sugar accumulation has also been shown to be spatiotemporally regulated in meristematic tissue in both the shoot and root apical meristem (Francis and Halford, 2006). Is the development of photosynthetic capacity in the rachis a cause of its early differentiation or a consequence of it? Does acquisition of photosynthetic capability and the production of sugars represent a global mechanism for signaling quiescent regions to progress into the cell division phase? More work exploring photosynthesis, sugar transport, hormone regulation, and gene expression will help uncover a possible role for the rachis in regulating morphogenetic processes during early leaf organogenesis.

The role of auxin presence as a possible defining mechanism in margin tissue organogenic potential

PIN1 directed auxin transport is widely accepted as an important regulator of leaf development (Reinhardt et al., 2003; Heisler et al., 2005; Scarpella and Helariutta, 2010; Kawamura et al., 2010; Hay and Tsiantis, 2006; Scarpella et al., 2006) and leaflet initiation (Koenig et al., 2009). A common mechanism unites *PIN1* directed development during leaf organogenesis across the systems studied - *PIN1* first directs auxin along the epidermal layer to sites of convergence on the meristem, then transports auxin subepidermally into internal layers (Scarpella et al., 2010). *PIN1* can be split into two highly supported sister clades; *PIN1* and *Sister of PIN1* (*SoPIN1*) (O'Connor et al., 2014; Bennett et al., 2014; Abraham Juárez et al., 2015). Recent work suggests the *SoPIN1* and *PIN1* clade may have disparate but complementary functions in auxin transport during organ initiation, where *SoPIN1* mainly functions in epidermal auxin flux to

establish organ initiation sites and *PIN1* functions in the transport of auxin inward (O'Connor et al., 2014; Abraham Juárez et al., 2015; Martinez et al., 2016). Tomato has one gene representative in the PIN1 clade *SlPIN1*, and in *SoPIN1* clade, two representatives; *SlSoPIN1a* (Solyc10g078370) and *SlSoPIN1b* (Solyc10g080880) (Pattison and Catalá, 2012; Nishio et al., 2010; Martinez et al., 2016). The results of our work suggest that in *tf-2, SlPIN1* is down-regulated at the region of leaflet initiation compared to wild type. Using *PIN1::GFP* as a reporter we observe a lack of fluorescence in the *tf-2* base marginal blastozone region (**Figure 9C-G**). Using DR5:VENUS as a reporter we see a diffuse localization of auxin in the base margin region of *tf-2* apices. Interestingly, even with external auxin applications, *tf-2* is not capable of leaflet initiation (Naz et al., 2013), suggesting that in *tf-2* the ability to direct auxin inwards using PIN1, and not auxin accumulation itself, may be compromised. It remains to be seen if this will be a common theme for organ formation in organisms where the PIN1 clade has diverged into two groups. Based on the results from the marginal blastozone region in *tf-2* we suggest that in addition to the creation of auxin foci, drainage of auxin into internal leaf layers may also be required for leaflet initiation. Analysis of higher order mutants in the larger *PIN1* clade should help resolve this issue.

Organogenic potential of the margin and homology of the leaf margin and the SAM

For this study we were especially interested in the genetic understanding of loss of organogenetic potential in the base margin of *tf-2*. We explicitly asked what the transcriptional differences are that explain loss of organogenetic potential in *tf-2* compared with wild type in specifically the margin base region. This led us to a small list of 23 genes differentially expressed genes that included *SlBOP2* (**Figure 10, Table 2**). Characterization of the *CR-bop2* line (**Figure 10**) revealed a phenotype of ectopic SAM production at the base of leaflets formation on the rachis of the complex leaf. This work provides support for the importance of the suppressive function of meristematic identity of the BOP family during leaf morphogenesis. BOP1 was introduced as a suppressor of lamina differentiation on the petiole of *Arabidopsis thaliana* simple leaves (Ha et al., 2003, 2004) functioning in limiting meristematic cells, as the *bop1* mutant displayed ectopic meristematic cells beyond the boundary between the base of the blade and petiole (Ha et al., 2003, 2004). Further work using *SlBOP* knockdowns and knockout lines demonstrated SlBOP2 function in suppressing organogenetic potential (S7 Figure; (Xu et al., 2016; Ichihashi et al., 2014), these lines with reduced or absent *SlBOP* function showed increase in leaflet organ initiation / leaf complexity. BOP is known to interact with transcription

factors to regulate floral identity including BOP interaction with PERIANTHIA (PAN) in *Arabidopsis (Hepworth and Pautot, 2015)* and TERMINATING FLOWER (TMF) interaction with *SlBOPs* to repress meristematic maturation in tomato flowers (MacAlister et al., 2012; Xu et al., 2016). We further hypothesize SlBOP2 and transcription factor interaction to regulate organogenic potential in complex leaves, possibly through direct binding of the TF transcription factor to the upstream regulatory region of *SlBOP2* (**Figure 10F**). We suggest both *TF and SlBOP2* function in suppressing meristematic properties of the margin during an early developmental window that is gradually closed with leaf maturation, an idea consistent with the view of the marginal blastozone as described by Hagemann, 1970.

While our understanding of the recruitment of genetic regulators in a spatiotemporal context grows, one of the more exciting questions still remains: is the marginal meristem evolutionarily derived from the SAM (Floyd and Bowman, 2010)? While ectopic adventitious shoot apical meristems have been shown to occur on leaves of functional knockouts of CUP-SHAPED-COTYLEDONS2 (CUC2) and CUC3 (Blein et al., 2008; Aichinger et al., 2012; Hibara et al., 2003) and in homeobox genes KNOTTED-1 (*KN1)* and *Arabidopsis Kn1-like* (*KNAT1*) gene overexpression lines (Chuck et al., 1996; Sinha and Hake, 1994), ectopic meristems at a region analogous to the base of an emerging leaflet, suggests developmental analogy, and possibly homology of to axillary meristems. Axillary meristems form on the adaxial surface at the boundary zone between leaf and SAM where SlBOP2 has already been shown to play a regulatory role in this process in tomato (Izhaki et al., 2018), Barley (*Hordeum vulgare*) (Tavakol et al., 2015; Dong et al., 2017), and Maize (*Zea mays*) (Dong et al., 2017). The CR-slbop2 ectopic meristem phenotype on the margin of tomato complex leaves suggests the recruitment of similar signals in the margin that may also be present during axillary meristem formation during leaf initiation processes. This study adds further evidence that the margin is analogous, and possibly homologous at the process level to the SAM. The leaf margin likely evolved from the genetic recruitment of similar regulatory factors, including BOP gene regulation, and reinforces the importance of reiteration of genetic mechanisms to establish distinct spatial identity in neighboring domains during plant development.

Conclusion

Our current understanding of the margin is laid on foundational work that defined the margin by explicitly tracking developmental landmarks (Avery, 1933; Poethig and Sussex, 1985a; Dolan

and Poethig, 1998; Wolf et al., 1986). Early literature defined the leaf primordium as broadly meristematic early in development with this meristematic potential getting restricted and gradually lost as the leaf develops (Foster, 1936; Hagemann and Gleissberg, 1996b; Sachs, 1969). Although such studies provide a roadmap for describing growth patterns in the margin, a major challenge is to understand how they are specified at the genetic level (Whitewoods and Coen, 2017; Coen et al., 2017) and how this fits with our interpretation of the recruitment of regulatory mechanisms suppressing margin morphogenetic potential leading to leaf evolution in seed plants from ancestral shoot systems. Plant development is reliant on reiterative patterning and leaf development is no exception. The genetic mechanisms regulating the modulation of leaf developmental programs are many, but this work and others suggest that we can interpret the evolutionary transition of ancestral shoot systems to the reiterated production of seed plant leaves as occurring partly by modulation of genetic mechanism that suppressed morphogenetic and organogenetic potential of meristematic regions of structures that eventually gave rise to leaves. Follow up work in more species is needed to understand both the evolutionarily conserved mechanisms and how these mechanisms were modulated to sculpt the diversity of leaf forms seen in nature.

MATERIALS AND METHODS

Plant growth and tissue embedding

Seeds of *tf-2* (LA0512) and the wild type background Condine Red (LA0533) were obtained from the Tomato Genetics Resource Center (TGRC). Seeds were sterilized with 50% bleach for two minutes and rinsed 10 times with distilled water to remove bleach. The seeds were then placed on moist paper towels in Phyotrays (Sigma-Aldrich) in dark conditions for two days. They were then moved to a growth chamber and allowed to germinate for four days before being moved to soil for 8 days of growth. Seedlings were grown for a total of 14 days. Generation of the transgenic DR5::Venus (*cv M82*) line was described in (Shani et al., 2010) and the *AtpPIN1::PIN1::GFP* (*cv Moneymaker)* was described in (Bayer et al., 2009).

Plants were collected in the afternoon and vacuum infiltrated for one hour in ice-cold 3:1 (100% EtOH: 100% Acetic Acid) fixative, then further fixed overnight at 4°C. Samples were washed three times in 75% EtOH and proceeded through an EtOH series on shaker for one hour at each step (75%, 85%, 95%, 100%, 100%, 100%) at room temperature and placed in 100%

overnight at 4°C. All ethanol solutions were made with 2X autoclaved diethylpyrocarbonate (DEPC) treated water. Tissue proceeded through a Xylene in EtOH series for two hours each (25%, 50%, 75%, 100%, 100%) on a shaker at room temperature. Tissue sat overnight at room temperature in 100% Xylene with 20-40 paraffin chips (paraplast x-tra, Thermo Fisher Scientific). Tissue was then incubated at 42°C until the paraffin dissolved. The paraffin:xylene solution was subsequently removed and replaced with 100% paraffin and changed twice daily for 3 days at 55°C. Tissue was then embedded using tools and surfaces that were washed with RNAseZap (Thermo Fisher Scientific) and DEPC. Embedded blocks were transversely sectioned at 5 to 7 µm thickness using a Leica RM2125RT rotary microtome (Leica Microsystems) on RNase-free polyethylene naphthalate PEN membrane slides (Leica). Slides were dried at room temperature and deparaffinized with 100% Xylene.

EdU Visualization

Cell division was visualized by fluorescent signal derived from EdU incorporation assay. During S-phase EdU is incorporated into cells (Kotogány et al., 2010)**.** Protocol was a modification of previously published protocols (Nakayama et al., 2014; Ichihashi et al., 2011) using Click-iT ® EdU Alexa Fluor® Imaging kit (Invitrogen). Seedlings were dissected under microscope at 14 days old removing older leaves. P4 leaf epidermis was nicked using an insect mounting needle to increase infiltration needed in subsequent steps. Plant apex was then incubated in water containing 10 µM edu solution for two hours. Samples were then washed in 1x phosphate-buffered saline solution (PBS, PH 7.4) and fixed in FAA under vacuum infiltration for 3 hours. After 3 h, the samples were fixed in 3.7% formaldehyde in PBS (pH 7.4) for 30 min and then washed three times in PBS with shaking. Alexa Fluor coupling to EdU was performed in dark following manufacturer's instructions. Photographs were taken using Zeiss LSM 710 Confocal Microscope with excitation wavelengths set at 488 and 420 nm.

Flow Cytometry and GUS Staining

Ploidy levels were measured using the ploidy analyzer PA-I (Partec) as described previously (Sugimoto-Shirasu et al., 2002). Fresh tissue was extracted from whole leaves in youngest leaf age (Day 8), while older stage tissue was extracted from both top and bottom sections of the leaf. The tissue was further chopped with a razor blade. Cystain extraction buffer (Partec) was used to release nuclei. The solution was further filtered through a CellTrics filter (Partec), and

stained with Cystain fluorescent buffer (Partec). A minimum of 4000 nuclei isolated from for each ploidy measurement. Flow cytometry experiments were repeated at least three times using independent biological replicates.

Histochemical localization of GUS activity was performed as previously described (Kang and Dengler, 2002). Representative images were chosen from >15 samples stained in three independent experiments.

Laser Capture Microdissection and RNA processing

Each tissue type was independently captured through serial sections using a Leica LMD6000 Laser Microdissection System (Leica Microsystems). Each biological replicate contained tissue collected from 5-8 apices. See **S1 Figure** for rules followed for identification and dissection of tissue regions that were isolated. Tissue was collected in lysis buffer from RNAqueous®-Micro Total RNA Isolation Kit (Ambion) and immediately stored at -80 °C. RNA extraction was performed using RNAqueous®-Micro Total RNA Isolation Kit (Ambion) following manufacturer's instructions. RNA was further amplified using WT-Ovation™ Pico RNA Amplification System (ver. 1.0, NuGEN Technologies Inc.). RNA was purified using RNAClean ® magnetic beads (Agencourt) and processed within one month of fixation to ensure RNA quality.

RNAseq libraries were created using the protocol detailed by Kumar and coworkers (Kumar et al., 2012), starting with the second strand synthesis step with the exception of the following changes: For second strand synthesis, 10µL of cDNA >250ng was added with 0.5µl of random primers and 0.5µl of dNTP. Sample were then heated at 80ºC for 2 min, 60ºC for 10 sec, 50ºC for 10 sec, 40ºC for 10sec, 30ºC for 10 sec and 4ºC for at least 2-5 min. We then combined 5 µl of 10x DNA pol buffer, 31µL water, and 2.5µL DNA Pol I on ice. The samples were further incubated at 16ºC for 2.5 hours. We continued with the published (Kumar et al., 2012) protocol starting with step 2.3 Bead purification of double stranded DNA. Libraries were quality checked and quantified using Bioanalyzer 2100 (Agilent) on RNA 6000 Pico Kit (Agilent) chips at the UC Davis Genome Center. Libraries were sequenced on three lanes using the HiSeq2000 Illumina Sequencer at the Vincent J Coates Genomics Sequencing Laboratory at UC Berkeley.

Read Processing and differential expression analysis

Quality filtering, N removal, and adaptor trimming was performed on data from each of the three Illumina sequencing lanes separately. We first performed N removal using read_N_remover.py. Sequences below a quality (phred) score of 20 without reducing the read to below 35bp. To remove adapter contamination we used adapterEffectRemover.py setting the minimum read length to 41. To assess quality control of reads after pre-processing of reads, we ran FASTQC (available at http://www.bioinformatics.bbsrc.ac.uk/projects/fastqc/) before and after pre-processing. To first filter out reads that were from chloroplast or mitochondrial sequence, all libraries were mapped using STAR 2.4.0(Dobin et al., 2013) to S.lycopersicum_AFYB01.1 mitochondrial sequence from NCBI, and NC_007898.3 chloroplast sequence from NCBI. Reads that did not map to either organelle were then mapped using STAR 2.4.0 to the ITAG3.10 Solanum lycopersicum genome where non-genic sequence was masked using the inverse coordinates of the ITAG3.10 gene model gff file. Bedtools (Quinlan, 2014) coverageBed was then used to count mapped reads, using a bed file generated from ITAG3.10 gene models. We built an online visualization tool for the community to manually explore the reads generated across the six tissue types in both wild type and *tf-2*: bit.ly/2kkxsFQ (Winter et al., 2007; Patel et al., 2012).

Read processing and differential expression were performed using R package edgeR (Robinson et al., 2010). Pairwise differential gene expression in each region along the proximal-distal axis was calculated in each proximal-distal region (top, middle, base) in separate analyses. Differential gene expression was determined using `exactTest()`, multiple testing correction was performed using the Benjamini–Hochberg procedure, and significance of differential expression was determined by a cutoff of FDR < 0.05. To estimate differential expression of genes across the entire marginal blastozone and rachis regions, we used an additive linear model where the proximal-distal axis was assigned as a blocking factor, which adjusts for differences between margin and rachis in top, middle, and base: `model.matrix(~Region + Tissue)`. For both pairwise and modelling analysis of differential expression, counts per million were calculated from raw reads and genes which had < 5 reads in 2 or more reps to remove low counts. We estimated common negative binomial dispersion and normalized counts based on the trimmed mean of M-value (TMM) method (Robinson and Oshlack, 2010) across all samples. Normalized Read count as caluculated by Counts Per Million (cpm) available as **Dataset S9**.

SOM clustering

In order to explore the genes that are the most variable across tissue, we started with the top 25% genes based on coefficient of variation, ratio of standard deviation compared to mean, from our count data. To remove differences in count between samples because of magnitude of gene expression data was scaled between 2 and -2 in each wild type and *tf-2* separately using the `scale()` function (Team, 2014). Hexagonal layout was used for all SOM clustering (Kohonen). For basic SOM analysis the `SOM()` function in each genotype separately, while superSOMs were performed using `superSOM()` in the Kohonen R package (Wehrens and Buydens, 2007). Training for both methods was performed in 100 iterations in which a-learning rate decreased from 0.05 to 0.01. Codebook vectors and distance plots of cluster assignments were further using the visualization functions in Kohonen R package (Wehrens and Buydens, 2007) and ggplot2 (Wickham, 2009). To ensure the major variance in gene expression patterns were defined by SOM clustering and to verify consistency in clustering, cluster assignments were projects onto PC space. All scripts used in clustering are available at github/iamciera/lcmProject (DOI upon publication).

AUTHOR CONTRIBUTIONS

Conceived and designed the experiments: CM, NS. Performed molecular experiments and plant characterizations: CM. Plant maintenance and phenotyping of *CR-bop2* lines: SL. Contributed plant lines, protocols, and/or reagents: NS, KS. Performed computational analysis: CM. Performed read mapping: MW. Analyzed the data: CM, NS, KS. Wrote the paper: CM, NS. Edited Paper: CM, NS, KS.

ACKNOWLEDGEMENTS

The UC Davis Tomato Genetics Resource Center provided tomato germplasm, AtpPIN1: PIN1: GFP and the DR5: VENUSx6 lines are gifts from Cris Kuhlemeier (University of Bern) and Naomi Ori (Hebrew University, Israel), respectively. We thank Zachary Lippman (Cold Spring Harbor Laboratory) for the *CR-slbop2* lines. We would also like to acknowledge Eddi Esteban, Asher Pasha, and Nicholas J. Provart for building the EFP browser. C.C.M. was supported by a National Science Foundation Graduate Research Fellowship (DGE-1148897), Katherine Esau Summer Fellowship, Walter R. and Roselinde H. Russell Fellowship, and Elsie Taylor Stocking Fellowship. Part of the work was supported by NSF PGRP grant IOS–0820854 (to N.R. S., Julin Maloof and Jie Peng). C.C.M. was also supported by a collaboration between

the National Science Foundation and the Japan Society for the Promotion of Science with a Graduate Research Opportunities Worldwide (GROW) award. This material is based upon work supported by the National Science Foundation under Award Numbers DBI-0735191, DBI-1265383, and DBI-1743442. URL: www.cyverse.org. We thank Daniel Chitwood (Michigan State University) who provided computational training and insightful discussion which greatly assisted the research and Kristina Zumstein (UC Davis) for her work and organization on several experiments. We would also like to thank Siobhan Brady (UC Davis) and Andrew Groover (USDA) for their helpful comments and John Harada (UC Davis) and Julie Pelletier (UC Davis) for use and training on the laser capture microdissection microscope.

DATASETS

S1_Dataset_allsig_DE_seperately.csv - Results of differential gene expression between margin and rachis in each of the top, middle, and base regions in both genotypes (WT and *tf-2)*

S2_Dataset_sig_go_terms.csv - GO terms describing DE expression performed between margin and rachis in each of the top, middle, and base regions in both genotypes (WT and *tf-2)*

S3_Dataset_wt_modelled_DE.txt - Performed with only wild type reads these are the Results from DE across the margin and rachis tissue and to adjust for variability between the proximal-distal axis, we employed an additive linear model using the top, middle, and base identities as a blocking factor in our experimental design.

S5_Dataset_top25_coefficent_of_variation.csv - Most variable genes across tissue we used the top 25% of genes based on coefficient of variation, resulting in a dataset of 6,582 unique genes.

S6_Dataset_wt_SOM_small_cluster_assignments.csv - SOM cluster assignments for wild type using a codemap vector of 6 illustrating the top six gene expression clusters.

S7_wt_SOM_small_sigGOterms.csv - GO terms derived from Dataset S6.

S8_wt_SOM_large_cluster_assignments.csv - SOM cluster analysis with a codemap vector of 36 in wild type.

S9_Dataset_normalizedReadCount_cpm.csv - Normalized Read counts calculated as counts per million (cpm).

S10_Dataset_tf2_modelled_DE.txt - Performed with only *tf-2* reads these are the Results from DE across the margin and rachis tissue and to adjust for variability between the proximal-distal axis, we employed an additive linear model using the top, middle, and base identities as a blocking factor in our experimental design.

955

SUPPLEMENTAL FIGURES

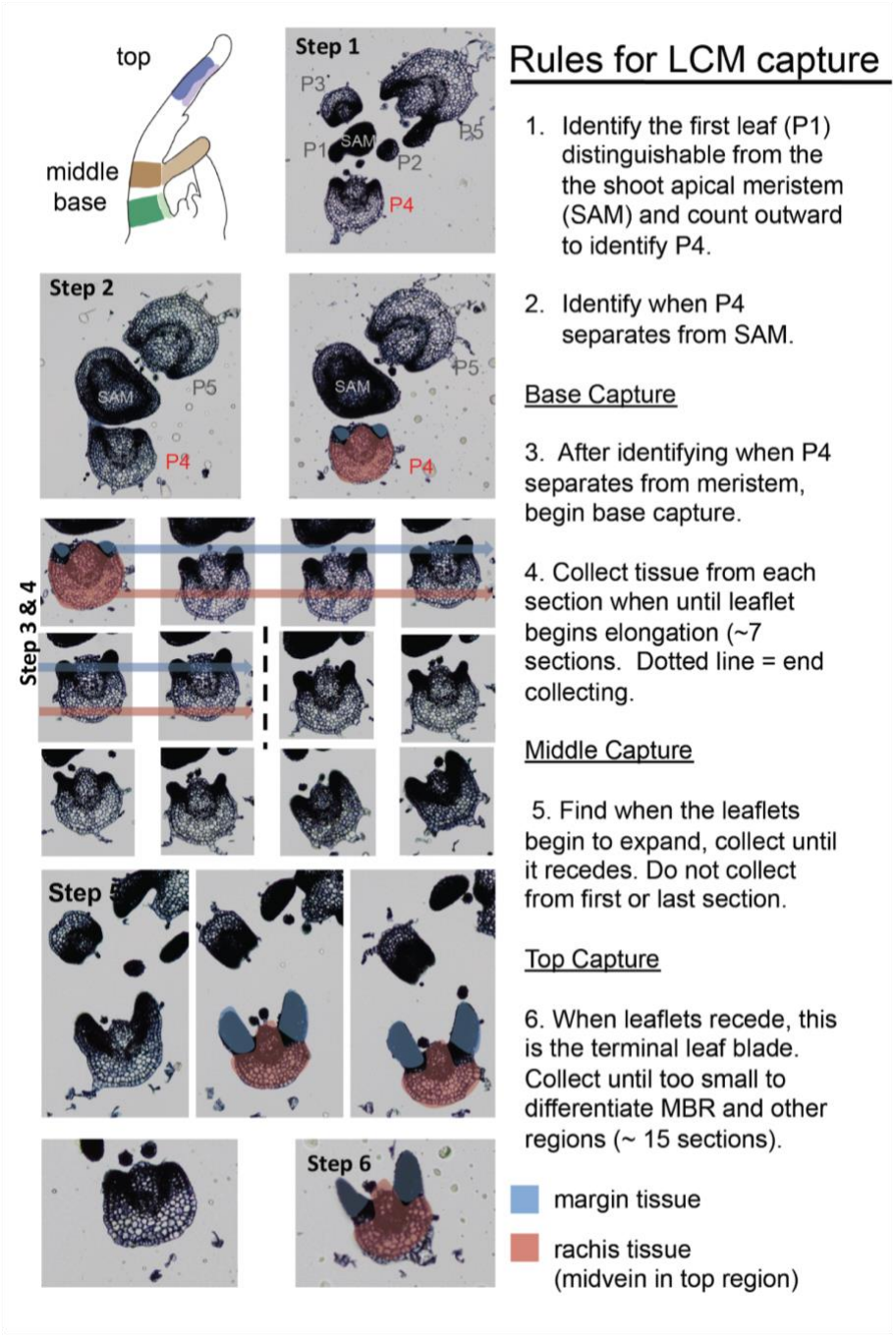

S1 Figure - Explicit Rules for Laser Capture Microdissection (LCM) tissue collection

Schematic and rules that were followed when making tissue collections using the LCM microscope.

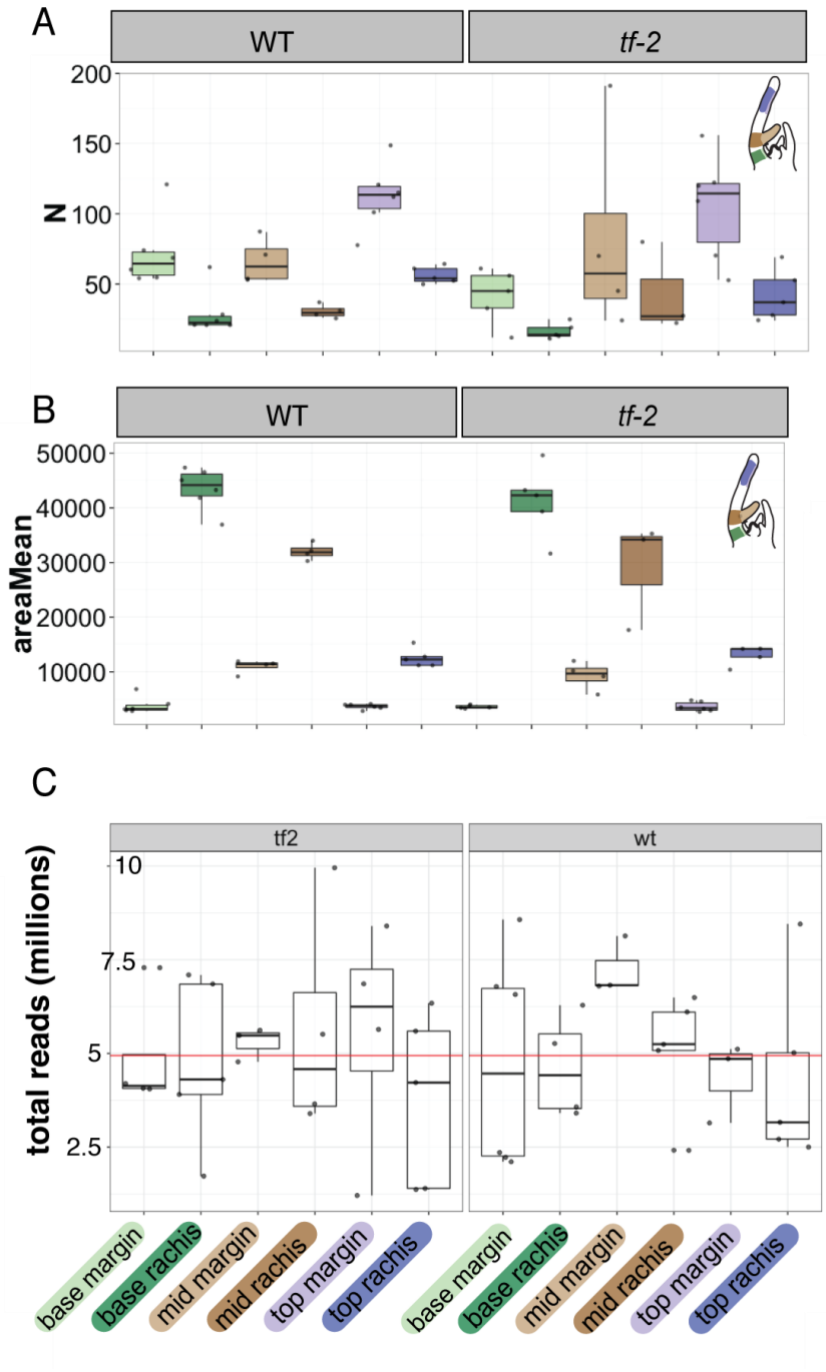

S2 Figure - Laser cutting necessary to achieve enough RNA for sequencing libraries and library reads achieved

The type and amount of tissue needed varied depending on cellular density and how much each developmental stage occurred on a P4 leaf primordiaBoxplots displaying the number of LCM (A) cuts and (B) area (μm) needed to per tissue sub-region to achieve enough tissue for RNA

970 amplification and Illumina sequencing. (C) Boxplot displaying the number of reads in each replicate.

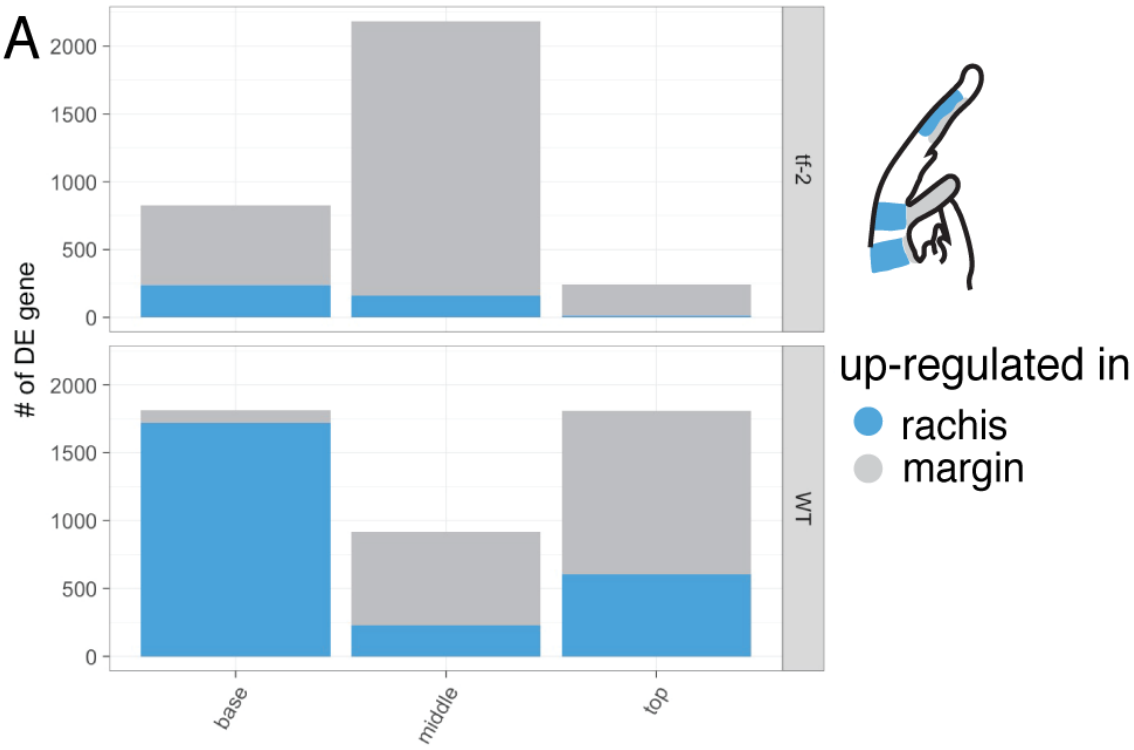

975 **S3 Figure - Summary of number of differential gene expression results in wild type and *tf-2***

(A) Bar graph displaying the number genes present in each of the differential expression results in wild type and *tf-2* margin vs rachis tissue. Each differential expression analysis was performed separately in each genotype and in each region (top, middle, and base) between the
980 margin and rachis.

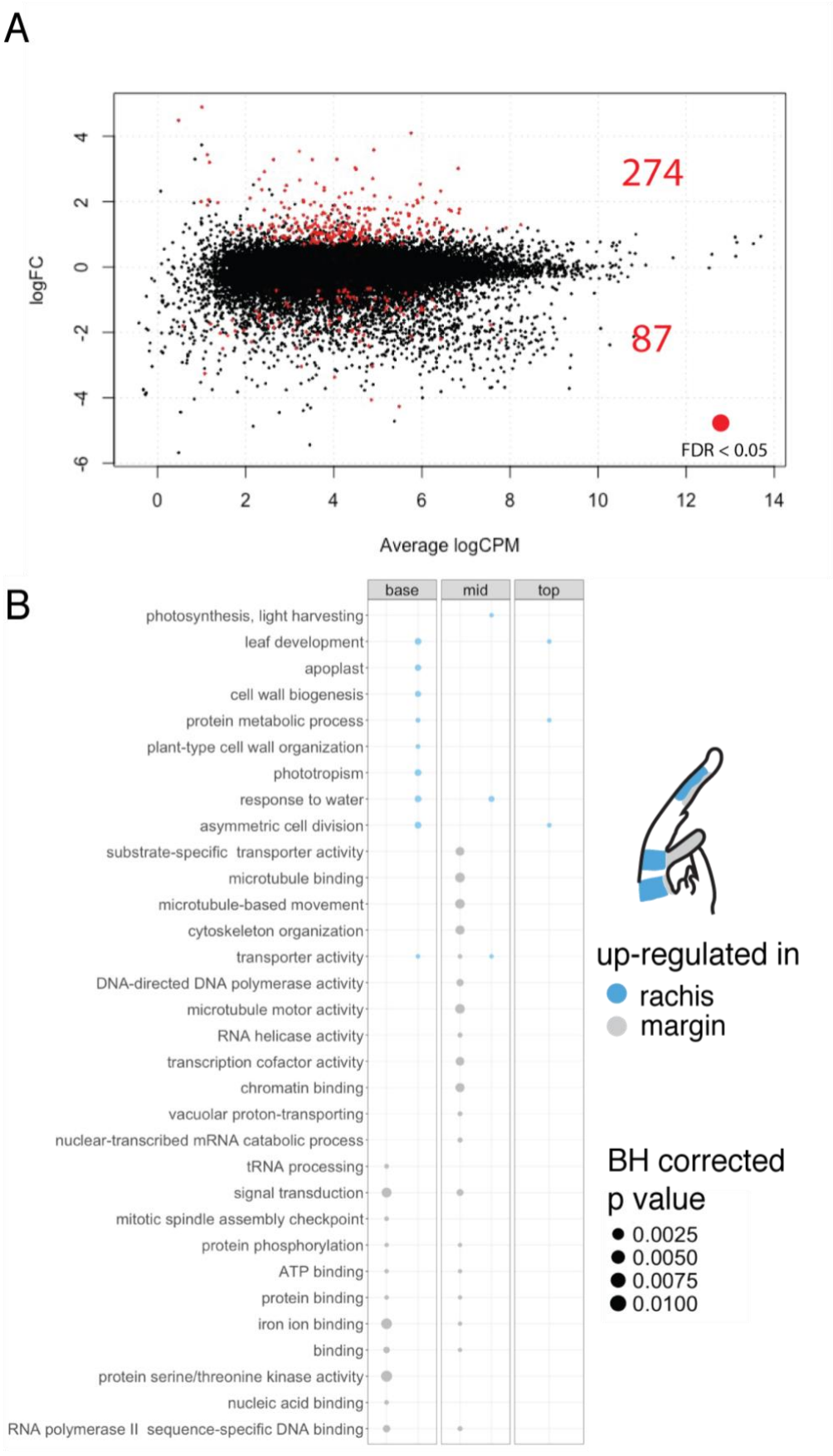

S4 Figure - Summary of differential expression in *tf-2* across the entire proximal distal axis

(A) Results from differential gene expression in *tf-2* displaying average log Counts Per Million (LogCPM) over log Fold Change (logFC), illustrating the number of significantly differentially regulated genes (red) between margin and rachis tissue when the top, middle, and base. (B) Pointplot displaying the summary of GO terms describing up-regulated genes in margin (grey) compared to rachis (blue). See **Dataset S10.**

A

	PC1	PC2	PC3	PC4	PC5	PC6
Standard deviation	1.3841	1.2535	1.0666	0.9009	0.7508	1.65E-15
Proportion of Variance	0.3193	0.2619	0.1896	0.1353	0.09395	0.00E+00
Cumulative Proportion	0.3193	0.5812	0.7708	0.9061	1	1.00E+00

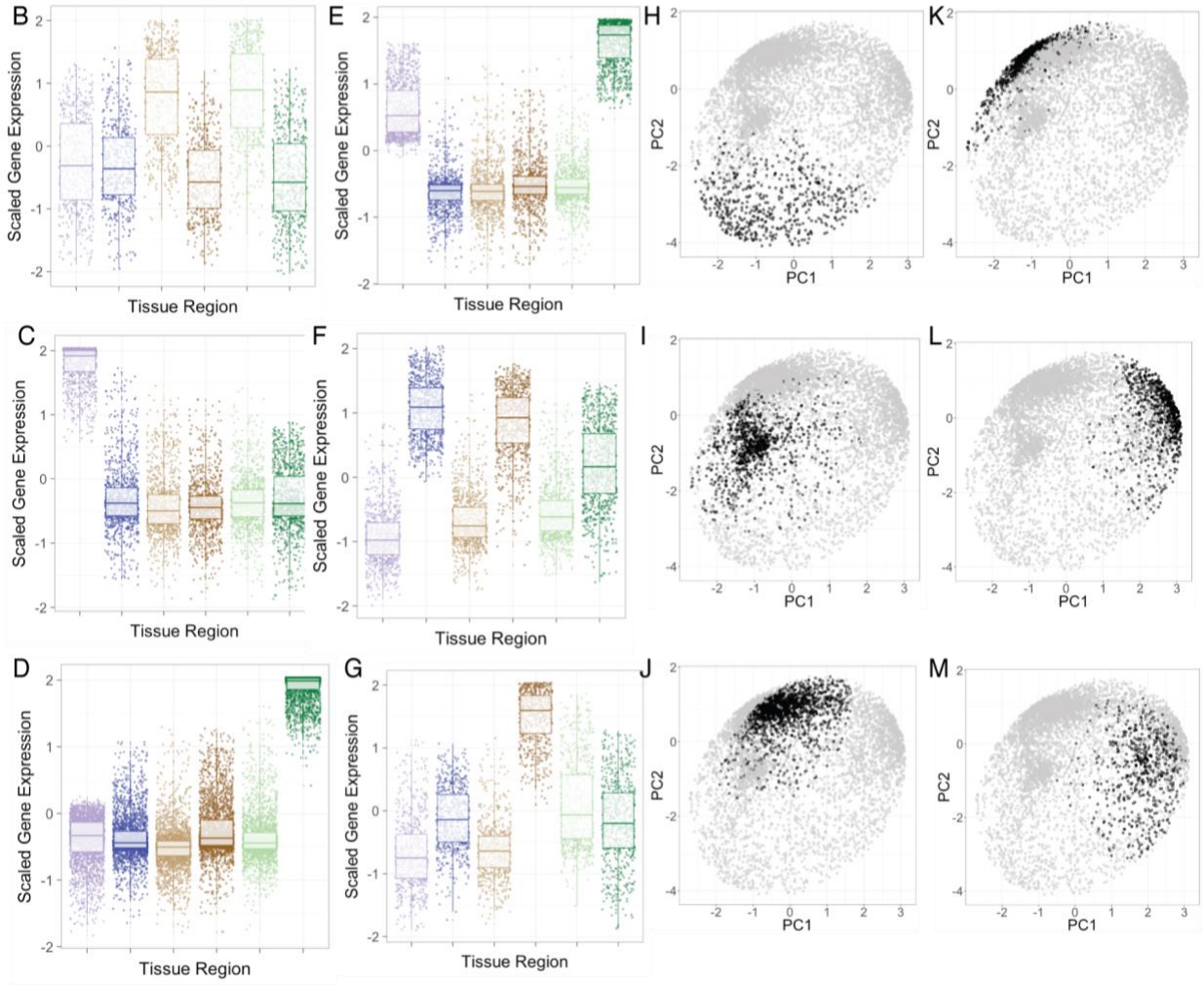

S5 Figure - Relationship between SOM clustering analysis and PCA analysis when performed on wild type genes across tissues

PCA was performed on normalized gene expression counts. SOM clustering was performed with the same normalized gene expression counts with defined clustering map size of six. (A) Statistics of PCA results. (B) - (G) summarizes each cluster, where each point represents a

gene in the cluster and its expression value across the six tissue regions. (H) - (M) Shows highlights each gene in PC space and the bold points reflect the genes present in each cluster in the SOM analysis.

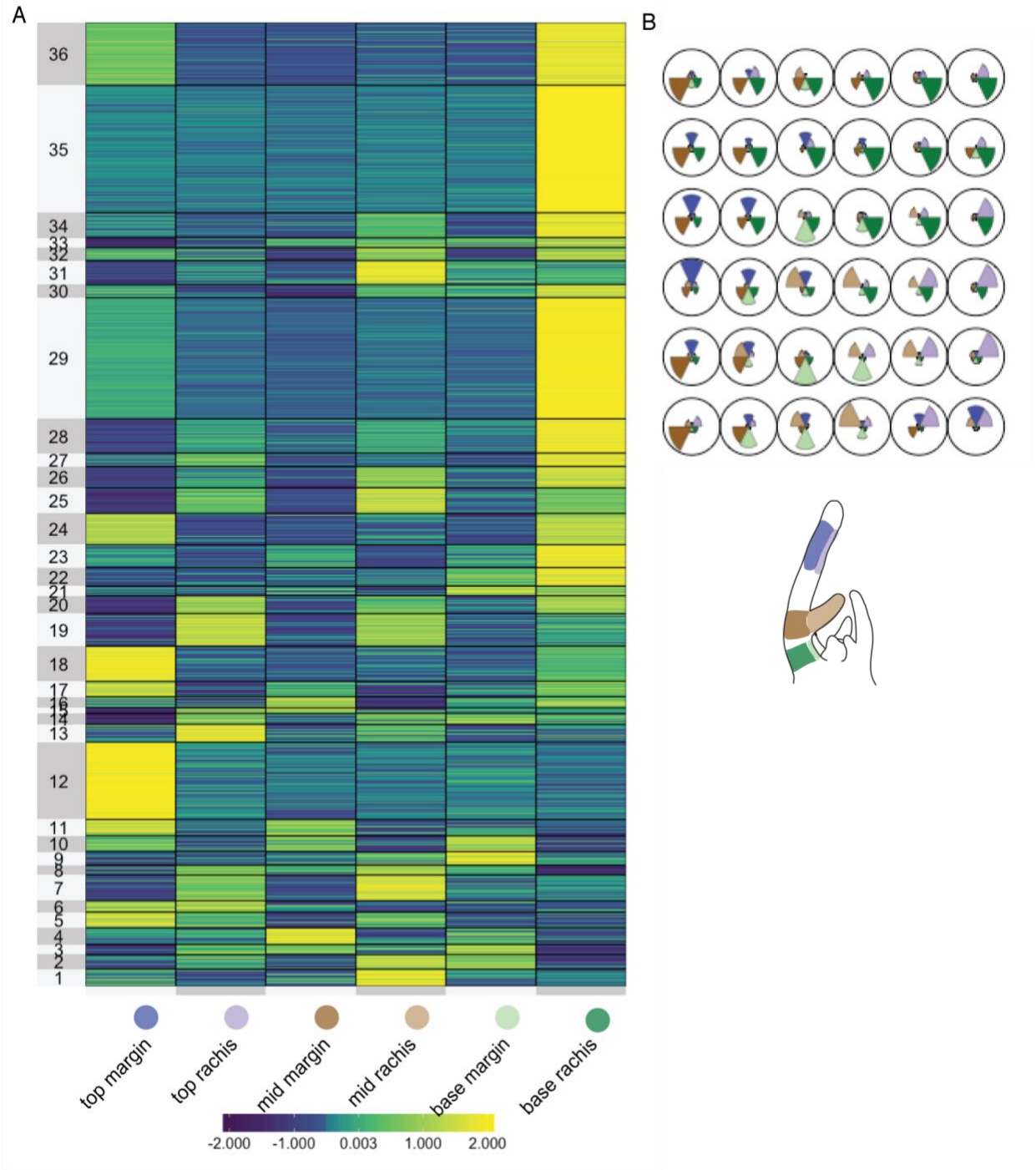

S6 Figure - Visualization of large SOM clustering analysis
(A) Heatmap representing the gene expression pattern of the 36 clusters of genes. (B) Codevector map displaying how much tissues expression in each region per gene contributed to cluster assignments.

S7 Figure

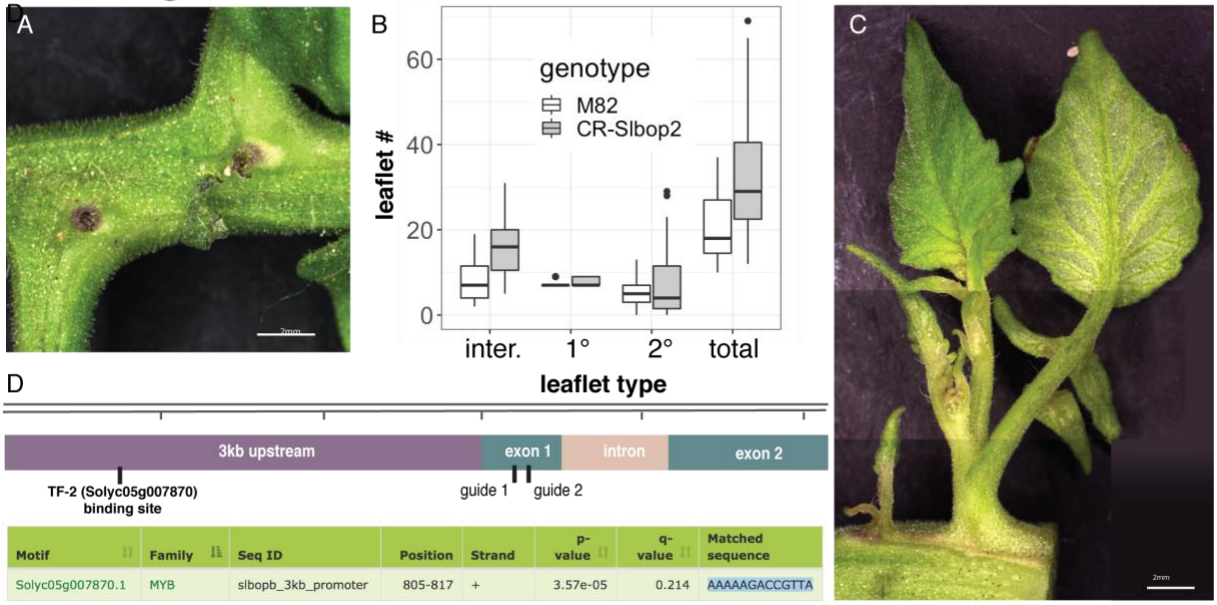

S7 Figure - *CR-slbop2* phenotyping and *SlBOP2* genomic map
(A) Scars of ectopic shoot apical meristem (SAM) tissue death at the leaflet nodes *CR-slbop2* leaves. (B) Leaf complexity counts in wild type (M82) and *CR-slbop2* plants (C) Example of an ectopic SAM that has proceeded in mature enough to contain complex leaves. (D) *SlBOP2* genomic region showing a TF-2 binding site and where the CRISPR guides are located that created the *CR-slbop2* line. Scale bar = 2mm in (A) and (C)

REFERENCES

Abraham Juárez, M.J., Hernández Cárdenas, R., Santoyo Villa, J.N., O'Connor, D., Sluis, A., Hake, S., Ordaz-Ortiz, J., Terry, L., and Simpson, J. (2015). Functionally different PIN proteins control auxin flux during bulbil development in Agave tequilana. J. Exp. Bot. **66**: 3893–3905.

Aichinger, E., Kornet, N., Friedrich, T., and Laux, T. (2012). Plant stem cell niches. Annu. Rev. Plant Biol. **63**: 615–636.

Andriankaja, M., Dhondt, S., De Bodt, S., Vanhaeren, H., Coppens, F., De Milde, L., Mühlenbock, P., Skirycz, A., Gonzalez, N., Beemster, G.T.S., and Inzé, D. (2012). Exit from proliferation during leaf development in Arabidopsis thaliana: a not-so-gradual process. Dev. Cell **22**: 64–78.

Avery, G.S. (1933). Structure and Development of the Tobacco Leaf. Am. J. Bot. **20**: 565–592.

Bayer, E.M., Smith, R.S., Mandel, T., Nakayama, N., Sauer, M., Prusinkiewicz, P., and Kuhlemeier, C. (2009). Integration of transport-based models for phyllotaxis and midvein formation. Genes Dev. **23**: 373–384.

Beemster, G.T.S., De Veylder, L., Vercruysse, S., West, G., Rombaut, D., Van Hummelen, P., Galichet, A., Gruissem, W., Inzé, D., and Vuylsteke, M. (2005). Genome-wide analysis of gene expression profiles associated with cell cycle transitions in growing organs of Arabidopsis. Plant Physiol. **138**: 734–743.

Bendahmane, A. and Theres, K. (2011). Shoot Branching and Leaf Dissection in Tomato Are Regulated by Homologous Gene Modules. Plant Cell: 1–16.

Benková, E., Michniewicz, M., Sauer, M., Teichmann, T., Seifertová, D., Jürgens, G., and Friml, J. (2003). Local, efflux-dependent auxin gradients as a common module for plant organ formation. Cell **115**: 591–602.

Bennett, T., Brockington, S.F., Rothfels, C., Graham, S., Stevenson, D., Kutchan, T., Rolf, M., Thomas, P., Wong, G.K.-S., Leyser, O., and Others (2014). Paralagous radiations of PIN proteins with multiple origins of non-canonical PIN structure. Mol. Biol. Evol.: msu147.

Bergervoet, J.H.W., Berhoeven, H.A., Gilissen, L.J.W., and Bino, R.J. (1996). High amounts of nuclear DNA in tomato (Lycopersicon esculentum Mill.) pericarp. Plant Sci. **116**: 141–145.

Bilsborough, G.D., Runions, A., Barkoulas, M., Jenkins, H.W., Hasson, A., Galinha, C., Laufs, P., Hay, A., Prusinkiewicz, P., and Tsiantis, M. (2011). Model for the regulation of Arabidopsis thaliana leaf margin development. Proc. Natl. Acad. Sci. U. S. A. **108**: 3424–3429.

Bläsing, O.E., Gibon, Y., Günther, M., Höhne, M., Morcuende, R., Osuna, D., Thimm, O., Usadel, B., Scheible, W.-R., and Stitt, M. (2005). Sugars and circadian regulation make major contributions to the global regulation of diurnal gene expression in Arabidopsis. Plant Cell **17**: 3257–3281.

Blein, T., Pulido, A., Vialette-Guiraud, A., Nikovics, K., Morin, H., Hay, A., Johansen, I.E., Tsiantis, M., and Laufs, P. (2008). A conserved molecular framework for compound leaf development. Science **322**: 1835–1839.

Bourdon, M., Frangne, N., Mathieu-Rivet, E., Nafati, M., Cheniclet, C., Renaudin, J.-P., and Chevalier, C. (2010). Endoreduplication and Growth of Fleshy Fruits. In Progress in Botany 71, U. Lüttge, W. Beyschlag, B. Büdel, and D. Francis, eds, Progress in Botany. (Springer Berlin Heidelberg), pp. 101–132.

Cheniclet, C., Rong, W.Y., Causse, M., Frangne, N., Bolling, L., Carde, J.-P., and Renaudin, J.-P. (2005). Cell expansion and endoreduplication show a large genetic variability in pericarp and contribute strongly to tomato fruit growth. Plant Physiol. **139**: 1984–1994.

Chuck, G., Lincoln, C., and Hake, S. (1996). KNAT1 induces lobed leaves with ectopic meristems when overexpressed in Arabidopsis. Plant Cell **8**: 1277–1289.

Coen, E., Kennaway, R., and Whitewoods, C. (2017). On genes and form. Development **144**: 4203–4213.

De Veylder, L., Larkin, J.C., and Schnittger, A. (2011). Molecular control and function of endoreplication in development and physiology. Trends Plant Sci. **16**: 624–634.

Dobin, A., Davis, C.A., Schlesinger, F., Drenkow, J., Zaleski, C., Jha, S., Batut, P., Chaisson, M., and Gingeras, T.R. (2013). STAR: ultrafast universal RNA-seq aligner. Bioinformatics **29**: 15–21.

Dolan, L. and Poethig, R. (1998). Clonal analysis of leaf development in cotton. Am. J. Bot. **85**: 315.

Dong, Z., Li, W., Unger-Wallace, E., Yang, J., Vollbrecht, E., and Chuck, G. (2017). Ideal crop plant architecture is mediated by tassels replace upper ears1, a BTB/POZ ankyrin repeat gene directly targeted by TEOSINTE BRANCHED1. Proc. Natl. Acad. Sci. U. S. A. **114**: E8656–E8664.

Donnelly, P.M., Bonetta, D., Tsukaya, H., Dengler, R.E., and Dengler, N.G. (1999). Cell cycling and cell enlargement in developing leaves of Arabidopsis. Dev. Biol. **215**: 407–419.

Efroni, I., Blum, E., Goldshmidt, A., and Eshed, Y. (2008). A protracted and dynamic maturation schedule underlies Arabidopsis leaf development. Plant Cell **20**: 2293–2306.

Eshed, Y., Baum, S.F., Perea, J.V., and Bowman, J.L. (2001). Establishment of polarity in lateral organs of plants. Curr. Biol. **11**: 1251–1260.

Floyd, S.K. and Bowman, J.L. (2010). Gene expression patterns in seed plant shoot meristems and leaves: homoplasy or homology? J. Plant Res. **123**: 43–55.

Foster, A.S. (1936). Leaf differentiation in angiosperms. Bot. Rev. **2**: 349–372.

Francis, D. and Halford, N.G. (2006). Nutrient sensing in plant meristems. Plant Mol. Biol. **60**: 981–993.

Gutierrez, C. (2005). Coupling cell proliferation and development in plants. Nat. Cell Biol. **7**: 535–541.

Ha, C.M., Jun, J.H., Nam, H.G., and Fletcher, J.C. (2004). BLADE-ON-PETIOLE1 encodes a BTB/POZ domain protein required for leaf morphogenesis in Arabidopsis thaliana. Plant Cell Physiol. **45**: 1361–1370.

Ha, C.M., Kim, G.-T., Kim, B.C., Jun, J.H., Soh, M.S., Ueno, Y., Machida, Y., Tsukaya, H., and Nam, H.G. (2003). The BLADE-ON-PETIOLE 1 gene controls leaf pattern formation through the modulation of meristematic activity in Arabidopsis. Development **130**: 161–172.

Hagemann, W. and Gleissberg, S. (1996a). Organogenetic capacity of leaves: The significance of marginal blastozones in angiosperms. Plant Syst. Evol. **199**: 121–152.

Hagemann, W. and Gleissberg, S. (1996b). Systematics and Evolution Organogenetic capacity of leaves : the significance of marginal blastozones in angiosperms. **199**: 121–152.

Hay, A. and Tsiantis, M. (2006). The genetic basis for differences in leaf form between Arabidopsis thaliana and its wild relative Cardamine hirsuta. Nat. Genet. **38**: 942–947.

Heisler, M.G., Ohno, C., Das, P., Sieber, P., Reddy, G.V., Long, J. a., and Meyerowitz, E.M. (2005). Patterns of auxin transport and gene expression during primordium development revealed by live imaging of the Arabidopsis inflorescence meristem. Curr. Biol. **15**: 1899–1911.

Hepworth, S.R. and Pautot, V.A. (2015). Beyond the Divide: Boundaries for Patterning and Stem Cell Regulation in Plants. Front. Plant Sci. **6**: 1052.

Hibara, K.-I., Takada, S., and Tasaka, M. (2003). CUC1 gene activates the expression of SAM-related genes to induce adventitious shoot formation. Plant J. **36**: 687–696.

Ichihashi, Y., Aguilar-Martínez, J.A., Farhi, M., Chitwood, D.H., Kumar, R., Millon, L.V., Peng, J., Maloof, J.N., and Sinha, N.R. (2014). Evolutionary developmental transcriptomics reveals a gene network module regulating interspecific diversity in plant leaf shape. Proc. Natl. Acad. Sci. U. S. A. **111**: E2616–21.

Ichihashi, Y., Kawade, K., Usami, T., Horiguchi, G., Takahashi, T., and Tsukaya, H. (2011). Key proliferative activity in the junction between the leaf blade and leaf petiole of Arabidopsis. Plant Physiol. **157**: 1151–1162.

Izhaki, A., Alvarez, J.P., Cinnamon, Y., Genin, O., Liberman-Aloni, R., and Eyal, Y. (2018). The Tomato BLADE ON PETIOLE and TERMINATING FLOWER Regulate Leaf Axil Patterning Along the Proximal-Distal Axes. Frontiers in Plant Science **9**.

Joubès, J., Chevalier, C., Dudits, D., Heberle-Bors, E., Inzé, D., Umeda, M., and Renaudin, J.-P. (2000). CDK-related protein kinases in plants. In The Plant Cell Cycle, D. Inzé, ed (Springer Netherlands), pp. 63–76.

Kang, J. and Dengler, N. (2002). Cell cycling frequency and expression of the homeobox gene ATHB-8 during leaf vein development in Arabidopsis. Planta **216**: 212–219.

Kawamura, E., Horiguchi, G., and Tsukaya, H. (2010). Mechanisms of leaf tooth formation in Arabidopsis. Plant J. **62**: 429–441.

Kidner, C.A. and Timmermans, M.C.P. (2007). Mixing and matching pathways in leaf polarity. Curr. Opin. Plant Biol. **10**: 13–20.

Koenig, D., Bayer, E., Kang, J., Kuhlemeier, C., and Sinha, N. (2009). Auxin patterns Solanum lycopersicum leaf morphogenesis. Development **136**: 2997–3006.

Kohonen, T. Self-organized formation of topologically correct feature maps. Biol. Cybern. **43**: 59–69.

Kondorosi, E., Roudier, F., and Gendreau, E. (2000). Plant cell-size control: growing by ploidy? Curr. Opin. Plant Biol. **3**: 488–492.

Kotogány, E., Dudits, D., Horváth, G.V., and Ayaydin, F. (2010). A rapid and robust assay for detection of S-phase cell cycle progression in plant cells and tissues by using ethynyl deoxyuridine. Plant Methods **6**: 5.

Kumar, R., Ichihashi, Y., Kimura, S., Chitwood, D.H., Headland, L.R., Peng, J., Maloof, J.N., and Sinha, N.R. (2012). A High-Throughput Method for Illumina RNA-Seq Library Preparation. Front. Plant Sci. **3**: 202.

Lastdrager, J., Hanson, J., and Smeekens, S. (2014). Sugar signals and the control of plant growth and development. J. Exp. Bot. **65**: 799–807.

Lilley, J.L.S., Gee, C.W., Sairanen, I., Ljung, K., and Nemhauser, J.L. (2012). An endogenous carbon-sensing pathway triggers increased auxin flux and hypocotyl elongation. Plant Physiol. **160**: 2261–2270.

Li, P. et al. (2010). The developmental dynamics of the maize leaf transcriptome. Nat. Genet. **42**: 1060–1067.

Liu, X.-D. and Shen, Y.-G. (2004). NaCl-induced phosphorylation of light harvesting chlorophyll a/b proteins in thylakoid membranes from the halotolerant green alga, Dunaliella salina. FEBS Lett. **569**: 337–340.

Ljung, K. (2013). Auxin metabolism and homeostasis during plant development. Development **140**: 943–950.

MacAlister, C.A., Park, S.J., Jiang, K., Marcel, F., Bendahmane, A., Izkovich, Y., Eshed, Y., and Lippman, Z.B. (2012). Synchronization of the flowering transition by the tomato TERMINATING FLOWER gene. Nat. Genet. **44**: 1393–1398.

Martinez, C.C., Koenig, D., Chitwood, D.H., and Sinha, N.R. (2016). A sister of PIN1 gene in tomato (Solanum lycopersicum) defines leaf and flower organ initiation patterns by maintaining epidermal auxin flux. Dev. Biol. **419**: 85–98.

Melaragno, J.E., Mehrotra, B., and Coleman, A.W. (1993). Relationship between Endopolyploidy and Cell Size in Epidermal Tissue of Arabidopsis. Plant Cell **5**: 1661–1668.

Mitra, A., Han, J., Zhang, Z.J., and Mitra, A. (2009). The intergenic region of Arabidopsis thaliana cab1 and cab2 divergent genes functions as a bidirectional promoter. Planta **229**: 1015–1022.

Moon, J. and Hake, S. (2011). How a leaf gets its shape. Curr. Opin. Plant Biol. **14**: 24–30.

Nakayama, H., Nakayama, N., Seiki, S., Kojima, M., Sakakibara, H., Sinha, N., and Kimura, S. (2014). Regulation of the KNOX-GA gene module induces heterophyllic alteration in North American lake cress. Plant Cell **26**: 4733–4748.

Naz, A.A., Raman, S., Martinez, C.C., Sinha, N.R., Schmitz, G., and Theres, K. (2013). Trifoliate encodes an MYB transcription factor that modulates leaf and shoot architecture in tomato. Proc. Natl. Acad. Sci. U. S. A. **110**: 2401–2406.

Nishio, S., Moriguchi, R., Ikeda, H., Takahashi, H., Takahashi, H., Fujii, N., Guilfoyle, T.J., Kanahama, K., and Kanayama, Y. (2010). Expression analysis of the auxin efflux carrier family in tomato fruit development. Planta **232**: 755–764.

O'Connor, D.L., Runions, A., Sluis, A., Bragg, J., Vogel, J.P., Prusinkiewicz, P., and Hake, S. (2014). A Division in PIN-Mediated Auxin Patterning during Organ Initiation in Grasses. PLoS Comput. Biol. **10**: e1003447.

Ori, N. et al. (2007). Regulation of LANCEOLATE by miR319 is required for compound-leaf development in tomato. Nat. Genet. **39**: 787–791.

Osuna, D., Usadel, B., Morcuende, R., Gibon, Y., Bläsing, O.E., Höhne, M., Günter, M., Kamlage, B., Trethewey, R., Scheible, W.-R., and Stitt, M. (2007). Temporal responses of transcripts, enzyme activities and metabolites after adding sucrose to carbon-deprived Arabidopsis seedlings. Plant J. **49**: 463–491.

Patel, R.V., Nahal, H.K., Breit, R., and Provart, N.J. (2012). BAR expressolog identification: expression profile similarity ranking of homologous genes in plant species. Plant J. **71**: 1038–1050.

Pattison, R.J. and Catalá, C. (2012). Evaluating auxin distribution in tomato (Solanum lycopersicum) through an analysis of the PIN and AUX/LAX gene families. Plant J. **70**: 585–598.

Poethig, R.S. and Sussex, I.M. (1985a). The cellular parameters of leaf development in tobacco: a clonal analysis. Planta **165**: 170–184.

Poethig, R.S. and Sussex, I.M. (1985b). The developmental morphology and growth dynamics of the tobacco leaf. Planta **165**: 158–169.

Price, J., Laxmi, A., St Martin, S.K., and Jang, J.-C. (2004). Global transcription profiling reveals multiple sugar signal transduction mechanisms in Arabidopsis. Plant Cell **16**: 2128–2150.

Quinlan, A.R. (2014). BEDTools: the Swiss-army tool for genome feature analysis. Curr. Protoc. Bioinformatics **47**: 11–12.

Reinhardt, D., Pesce, E.-R., Stieger, P., Mandel, T., Baltensperger, K., Bennett, M., Traas, J., Friml, J., and Kuhlemeier, C. (2003). Regulation of phyllotaxis by polar auxin transport. Nature **426**: 255–260.

Riou-Khamlichi, C., Menges, M., Healy, J.M., and Murray, J.A. (2000). Sugar control of the plant cell cycle: differential regulation of Arabidopsis D-type cyclin gene expression. Mol. Cell. Biol. **20**: 4513–4521.

Robinson, M.D., McCarthy, D.J., and Smyth, G.K. (2010). edgeR: a Bioconductor package for differential expression analysis of digital gene expression data. Bioinformatics **26**: 139–140.

Robinson, M.D. and Oshlack, A. (2010). A scaling normalization method for differential expression analysis of RNA-seq data. Genome Biol. **11**: R25.

Robinson, R. and Rick, C.M. (1954). New Tomato Seedling Characters and Their Linkage Relationships.

Sachs, T. (1969). Regeneration experiments on the determination of the form of leaves. Israel J Bot.

Sairanen, I., Novák, O., Pěnčík, A., Ikeda, Y., Jones, B., Sandberg, G., and Ljung, K. (2012). Soluble

carbohydrates regulate auxin biosynthesis via PIF proteins in Arabidopsis. Plant Cell **24**: 4907–4916.

Scarpella, E., Barkoulas, M., and Tsiantis, M. (2010). Control of leaf and vein development by auxin. Cold Spring Harb. Perspect. Biol. **2**: a001511.

Scarpella, E. and Helariutta, Y. (2010). Vascular pattern formation in plants. Curr. Top. Dev. Biol. **91**: 221–265.

Scarpella, E., Marcos, D., Friml, J., and Berleth, T. (2006). Control of leaf vascular patterning by polar auxin transport. Genes Dev. **20**: 1015–1027.

Shani, E., Ben-Gera, H., Shleizer-Burko, S., Burko, Y., Weiss, D., and Ori, N. (2010). Cytokinin regulates compound leaf development in tomato. Plant Cell **22**: 3206–3217.

Sinha, N. and Hake, S. (1994). The Knotted leaf blade is a mosaic of blade, sheath, and auricle identities. Dev. Genet. **15**: 401–414.

Skirycz, A., Claeys, H., De Bodt, S., Oikawa, A., Shinoda, S., Andriankaja, M., Maleux, K., Eloy, N.B., Coppens, F., Yoo, S.-D., and Others (2011). Pause-and-stop: the effects of osmotic stress on cell proliferation during early leaf development in Arabidopsis and a role for ethylene signaling in cell cycle arrest. Plant Cell **23**: 1876–1888.

Stokes, M.E., Chattopadhyay, A., Wilkins, O., Nambara, E., and Campbell, M.M. (2013). Interplay between sucrose and folate modulates auxin signaling in Arabidopsis. Plant Physiol. **162**: 1552–1565.

Sugimoto-Shirasu, K. and Roberts, K. (2003). “Big it up”: endoreduplication and cell-size control in plants. Curr. Opin. Plant Biol. **6**: 544–553.

Sugimoto-Shirasu, K., Stacey, N.J., Corsar, J., Roberts, K., and McCann, M.C. (2002). DNA topoisomerase VI is essential for endoreduplication in Arabidopsis. Curr. Biol. **12**: 1782–1786.

Sussex, I.M. and Kerk, N.M. (2001). The evolution of plant architecture. Curr. Opin. Plant Biol. **4**: 33–37.

Tamayo, P., Slonim, D., Mesirov, J., Zhu, Q., Kitareewan, S., Dmitrovsky, E., Lander, E.S., and Golub, T.R. (1999). Interpreting patterns of gene expression with self-organizing maps: methods and application to hematopoietic differentiation. Proc. Natl. Acad. Sci. U. S. A. **96**: 2907–2912.

Tavakol, E. et al. (2015). The barley Uniculme4 gene encodes a BLADE-ON-PETIOLE-like protein that controls tillering and leaf patterning. Plant Physiol. **168**: 164–174.

Team, R.C. (2014). A language and environment for statistical computing. R Foundation for Statistical Computing, Vienna.

Tindamanyire, J.M., Townsley, B., Kiggundu, A., Tushemereirwe, W., and Sinha, N. (2013). Building a bi-directional promoter binary vector from the intergenic region of Arabidopsis thaliana cab1 and cab2 divergent genes useful for plant transformation. Afr. J. Biotechnol. **12**: 1203–1208.

Tsukaya, H. (2014). Comparative leaf development in angiosperms. Curr. Opin. Plant Biol. **17**: 103–109.

Usadel, B., Bläsing, O.E., Gibon, Y., Retzlaff, K., Höhne, M., Günther, M., and Stitt, M. (2008). Global transcript levels respond to small changes of the carbon status during progressive exhaustion of carbohydrates in Arabidopsis rosettes. Plant Physiol. **146**: 1834–1861.

Wehrens, R. and Buydens, L. (2007). Self- and Super-organizing Maps in R: The kohonen Package. J. Stat. Softw. **21**: 1–19.

Whitewoods, C.D. and Coen, E. (2017). Growth and Development of Three-Dimensional Plant Form.

Curr. Biol. **27**: R910–R918.

Wickham, H. (2009). ggplot2: elegant graphics for data analysis (Springer Science & Business Media).

Wind, J., Smeekens, S., and Hanson, J. (2010). Sucrose: metabolite and signaling molecule. Phytochemistry **71**: 1610–1614.

Winter, D., Vinegar, B., Nahal, H., Ammar, R., Wilson, G.V., and Provart, N.J. (2007). An "Electronic Fluorescent Pictograph" Browser for Exploring and Analyzing Large-Scale Biological Data Sets. PLoS ONE **2**: e718.

Wolf, S.D., Silk, W.K., and Plant, R.E. (1986). QUANTITATIVE PATTERNS OF LEAF EXPANSION: COMPARISON OF NORMAL AND MALFORMED LEAF GROWTH IN VITIS VINIFERA CV. RUBY RED. Am. J. Bot. **73**: 832–846.

Xu, C., Park, S.J., Van Eck, J., and Lippman, Z.B. (2016). Control of inflorescence architecture in tomato by BTB/POZ transcriptional regulators. Genes Dev. **30**: 2048–2061.